様式6

論　文　目　録

報告番号	甲 工 乙 工 第 185 号 工 修	氏　名	直井　弘之
学位論文題目	Growth and Characterization of InNAs		

論文の目次

参考論文
主論文

"MOCVD GROWTH OF InAsN FOR INFRARED APPLICATIONS"
HIROYUKI NAOI, YOSHIKI NAOI and SHIRO SAKAI
Solid State Electronics 41, (1997) 319.

"Heteroepitaxial growth of InAs by low-pressure metalorganic chemical vapor deposition employing in situ generated arsine radicals"
H. Naoi, D. M. Shaw, G. J. Collins and S. Sakai
Journal of Crystal Growth 219, (2000) 481.

"Growth of InNAs by low pressure metalorganic chemical vapor deposition employing microwave-cracked nitrogen and in-situ generated arsine radicals"
H. Naoi, D. M. Shaw, Y. Naoi, G. J. Collins and S. Sakai
Journal of Crystal Growth (掲載決定).

副論文

"Growth of InNAs on GaAs(100) substrates by molecular-beam epitaxy"
Shiro Sakai, Tin S. Cheng, Thomas C. Foxon, Tomoya Sugahara, Yoshiki Naoi,
Hiroyuki Naoi
Journal of Crystal Growth 189/190, (1998) 471.

様式7

論　文　内　容　要　旨

報告番号	甲　工 乙　工　第 185 号 工　修	氏　　名	直井　弘之
学位論文題目	Growth and Characterization of InNAs		

内容要旨

本研究では，新しいIII-V族化合物半導体であるInN_xAs_{1-x}の結晶成長実験を行なった．V族側元素として窒素とそれ以外の原子を含む材料（例えば，GaN_xP_{1-x}やGaN_xAs_{1-x}などのIII-N-V混晶）では，バンドギャップエネルギーが大きなボーイングをもつなどの特徴が予期されている．すべてのIII-N-V混晶の中で，InN_xAs_{1-x}は一番小さなバンドギャップエネルギーを持ち，中間窒素固相比においては負のバンドギャップエネルギーを持つ可能性も予期されている．InN_xAs_{1-x}は，赤外線用の材料として有望であり，$Cd_xHg_{1-x}Te$，$Sn_xPb_{1-x}Te$，$InAs_xSb_{1-x}$，$Ga_xIn_{1-x}P_yAs_{1-y}$などの従来の赤外線用材料に取って代われるものであると考えられる．InNAsはIII-V族窒化物半導体デバイス上の低抵抗オーミック電極用材料としても興味深いものである．InNAsは研究テーマとして興味深いものであるが，GaNPやGaNAsほど研究されてはいない．本研究では，さまざまな成長法を用いて，(100)GaAs基板上InNAs結晶成長を試み，以下の結果が得られた．

まず，アンモニアを窒素源として用いた有機金属気相成長法（MOCVD法）によりInN_xAs_{1-x}（$x=0$~0.061）が得られた．InNAsのバンドギャップエネルギーは窒素の固相比が大きくなるほど小さくなった．$InN_{0.061}As_{0.939}$のバンドギャップエネルギーとして0.12eVという値が得られた．この値は，従来のIII-V族化合物半導体の中で，$InAs_xSb_{1-x}$を用いて得られたバンドギャップエネルギーの最小値0.10eVに匹敵するものである．この成長法では，窒素の固相比を大きくすることはできなかった．InNAsの成長温度におけるアンモニアの低熱分解効率が低窒素固相比の原因であることを明らかにした．

次に，プラズマ支援MOCVD法による成長を試みた．窒素ガスを窒素源として用い，マイクロ波プラズマを起こすことによりすべての原料ガスを混合したものを基板の上流で分解した．これは，窒素の固相比の大きな均質なInNAsを成長させることを目的とした．しかし，結晶化したInNAsを得ることはできなかった．同成長法によりInNの成長も試みたが，膜質はきわめてアモルファスに近いものであった．気相中の活性種間での化学反応が，膜質が悪いことの原因であると結論された．

続いて，分子線エピタキシー法（MBE）において，V族原料比N/Asを調整することにより，GaAs成長基板に格子整合した$InN_{0.38}As_{0.62}$の作成に成功した．成長層は相分離し，膜中にInAsが含まれていた．

最後に，上に示したプラズマ支援MOCVD法での反省をふまえ，気相中での化学反応を抑制することを目的として，窒素ラジカルを他のガスと混ぜずにMOCVD反応炉に導入することにより結晶成長を試みた．この成長法では，低生成率プラズマ生成アルシンをAsの原料として用いた．これは，V族原料比N/Asを大きくすることにより，窒素の固相比の大きなInNAsを作成することを目的とした．InN_xAs_{1-x}（$x=0.06$~0.13）を得ることができたが，成長層はいずれも相分離を起こし，膜中にウルツァイト構造InNを含んでいた．ウルツァイト構造InNが形成されたのは，成長開始直前の基板表面の窒化が原因であると指摘した．また，このプラズマ生成アルシンを用いてInAs単結晶膜作成に成功した．

Growth and Characterization of InNAs

March 2001

Hiroyuki Naoi

Growth and Characterization of InNAs

Dissertation Submitted in Candidacy for
the Degree of Ph. D.
by

Hiroyuki Naoi

Doctor Course in Materials Science and Engineering

Graduate School of Engineering

The University of Tokushima, Japan

March 2001

Abstract

In this doctoral study, the growth of a new III-V compound semiconductor material, InN_xAs_{1-x}, is investigated. Materials which include nitrogen and other group V elements as the anions (e.g., III-N-V alloys such as GaN_xP_{1-x}, GaN_xAs_{1-x}) are expected to have very unique properties such as large band gap energy bowing. Among the III-N-V alloys, InN_xAs_{1-x} is expected to produce the narrowest band gap energy, possibly even negative around mid-nitrogen composition. InN_xAs_{1-x} is a promising material for infrared (IR) applications, and may be an alternative to all the conventional IR materials such as $Cd_xHg_{1-x}Te$, $Sn_xPb_{1-x}Te$, $InAs_xSb_{1-x}$ and $Ga_xIn_{1-x}P_yAs_{1-y}$. Additionally, InNAs is interesting for low resistivity Ohmic contacts on III-V nitride devices as well. While many interesting points remain in the study of InNAs, this material has been relatively unstudied as compared to GaNP and GaNAs. Several growth methods have been tested for the growth of InNAs on a (100)GaAs substrate over the course of this doctoral study and the results are covered herein.

First, InN_xAs_{1-x} (x = 0~0.061) was obtained by conventional metalorganic chemical vapor deposition (MOCVD) using ammonia as the nitrogen source. The band gap energy of InNAs decreased with increase in the nitrogen solid phase composition. The band gap energy of $InN_{0.061}As_{0.939}$ was around 0.12 eV, which is comparable to the minimum band gap of 0.10 eV achieved in the $InAs_xSb_{1-x}$ material system among all the conventional III-V semiconductors. The low nitrogen composition of the grown InNAs was attributed to low pyrolysis efficiency of NH_3 in the range of InNAs growth temperatures.

Second, a plasma-assisted MOCVD growth technique was tested. Nitrogen gas was used as the nitrogen source, and all the mixed source gases were cracked by microwave excitation upstream of the growth substrate in an attempt to grow InNAs with higher nitrogen composition and good compositional uniformity. However, no crystallized InNAs was obtained. The growth of InN was also performed, again resulting in almost amorphous properties of the grown layer. These poor results were

attributed to the gas phase chemical reactions between activated source species.

Third, $InN_{0.38}As_{0.62}$ lattice-matched to (100)GaAs was grown by moleculer beam epitaxy (MBE) by adjusting the flux ratio of N/As. The grown layer included phase-separated InAs.

Finally, the separate production and introduction of nitrogen radicals into an MOCVD growth chamber, without mixing, were employed to suppress possible gas phase chemical reactions. A low production rate, plasma-based arsine generator was used to increase the N/As source ratio with the goal of synthesizing InNAs with a high nitrogen solid phase composition. InN_xAs_{1-x} (x = 0.06~0.13) phases were obtained. The grown InNAs layer was always accompanied by wurtzite InN. The occurrence of the phase-separated InN was attributed to GaAs substrate nitridation before the growth process initiation. Single crystalline InAs films were also obtained using the same arsine source.

Acknowledgments

Looking back on my doctoral student life of almost six years (three years at the University of Tokushima and almost three years at Colorado State University), I have been obliged to many people. Herein, I would like to express my gratitude to them.

I would like to express my great gratitude to Professor Shiro Sakai, my advisor, for introducing this interesting topic for my doctoral study, carrying out MBE growth of InNAs at the University of Nottingham in the United Kingdom of Great Britain and Northern Ireland, giving me an opportunity to study at Colorado State University in the United States of America, and guiding me from my graduation study through this doctoral study. His attitude to the scientific research, i.e., always seeking a new or original scientific topic which would bring advantages to our world, energetically approaching each issue in the research, and praising other's original works made deep and strong impressions on me. His attitudes influenced and developed my philosophy of research.

I wish to thank Professor Yoshihiro Shintani, a member of my thesis committee, for his useful comments and careful reading of the dissertation. Especially I am grateful to Professor Yoshihiro Shintani for his encouragement from my graduation study through this doctoral study.

I wish to thank Professor Tatsuo Kanashiro, a member of my thesis committee, for his useful comments and careful reading of the dissertation.

I would like to express my great gratitude to Professor George J. Collins of Colorado State University for kindly opening a place in his laboratory for my doctoral study and encouraging me not only during my stay at Colorado State University but also after I got back to the University of Tokushima. I am also grateful to Professor George J. Collins for allowing me to attend his class on the gas plasma. He was always creating new ideas in his research. He was always teaching the students courteously and opening his office door for the students all the time. His attitudes as well as his elaborately written lecture notes on plasmas made deep impressions on me.

I would like to express my great gratitude to Professor Thomas C. Foxon of the University of Nottingham for providing, in his laboratory, the MBE growth system for InNAs growth.

I would like to express my great gratitude to Doctoral student Denis M. Shaw of Colorado State University. He is the organizer of Professor Collins' laboratory. Although he was very busy managing the laboratory and taking care of other students, he listened and replied to my opinions, requests for the growth experiment apparatus and my questions on the plasma, every time courteously. I learned a lot not only about the plasma but also about mountain climbing from him. He saved my life in Colorado. After I got back to the University of Tokushima, he continuously encouraged me and assisted me in writing technical English when submitting papers to journals through this doctoral dissertation. I can not be too thankful to him. His energetic attitude, of never giving up, to the scientific research as well as his leadership in the laboratory made deep impressions on me.

I am grateful to Lecturer Yoshiki Naoi for his guidance from my master's study through this doctoral study and for his encouragement and help. His careful and precise approach to each issue in the scientific research made a deep impression on me.

I wish to thank Doctor Tin S. Cheng of the University of Nottingham (now working at University College London) for his technical assistance in the operation of MBE growth system.

I wish to thank Doctor Zeng-Qi Yu of Storage Technology Co. for his technical assistance in the operation of the arsine generation apparatus, and his encouragement and discussions during my stay in Colorado State University.

I wish to thank Doctoral student Hisao Sato (now, Doctor of Engineering, working for Nitride Semiconductor Co., Ltd.) for kindly providing me with his data on the pyrolysis of ammonia that was taken after a long period of operation time, and for his encouragement.

I wish to thank Doctoral student Jie Bai and Doctor Li Hongdong for transmission electron microscopy (TEM) measurements of a sample.

I wish to thank Assistant Nan Jiang (Administrator of the TEM apparatus) for his help in the TEM measurements.

I wish to thank Master student Takashi Nakanishi for energy dispersive x-ray spectroscopy (EDX) measurements of a sample.

I wish to thank Lecturer Katsushi Nishino and Technician Takeshi Inaoka for their helps and encouragements.

I would like to express my great gratitude to Sayuri M. Collins (Professor George J. Collins' wife). I stayed at the Collins home for the first year when I began to

study at Colorado State University. She kindly provided me a room in her house and cooked extra dinner for me everyday though she was very busy in taking care of her five kids. After I moved to the international house of Colorado State University, she continuously encouraged me and invited me to dinner party held in her house every time. She is Master of English Education. I learned a lot about how to study English conversation as well as American life from her. Without her help, my study in Colorado would not have been completed.

I wish to thank Mary Casey of Engineering Research Center of Colorado State University for her help and daily encouragements.

A part of this work was done by Master students Takashi Tomoyasu (now, Master of Engineering, working for New Japan Radio Co., Ltd.) and Kenji Iwaki (now, Master of Engineering, working for Obayashi Co.), and Bachelor students Tomoya Sugahara (now, Doctoral student at the University of Tokushima) and Keizo Kobatake (now, Graduate of Engineering, working for Chugoku Regional Bureau of Postal Service). I would like to thank them.

I especially wish to thank Doctoral student Satoshi Kurai (now, Doctor of Engineering, working at the University of Yamaguchi) for his help in my study from the beginning of my student life at the University of Tokushima through the research life at Sakai laboratory and for his encouragement.

I wish to thank all the other members of Sakai laboratory and satellite venture business laboratory of the University of Tokushima in the past and the present for their friendly help.

I would like to thank the staff of the University of Tokushima for their helps in paperwork when I moved to Colorado State University.

A part of my doctoral student life and the research expenses were financially supported by the Japan Society for the Promotion of Science. I would like to express my appreciation to the organization herein.

Finally, I would like to express my faithful appreciation to my parents for their financial support and occasional encouragement throughout my long student life.

Contents

Chapter 1
Introduction

1-1 Background

The success of GaN-based short wavelength devices [1] such as blue light emitting diodes (LEDs) [2-4] and violet laser diodes (LDs) [5,6] have made nitrogen a new element for device quality compound semiconductor materials. Most of the GaN-related work so far has been on the AlGaInN material system, in which nitrogen was only an anion. The band lineup of AlN/GaN/InN interfaces are predicted to be type I, and the band gap bowing of these alloys is relatively small [7].

In recent years, another type of group III-V compound semiconductor material which includes nitrogen and other group V elements as the anions (III-N-V alloys) has attracted much interest and is increasingly studied. These are, for example, GaN_xP_{1-x} [8-16], GaN_xAs_{1-x} [17-25] and $Ga_xIn_{1-x}N_yAs_{1-y}$ [26, 27] alloys. These alloys are very different from AlGaInN material system. III-N-V alloys are expected to have very unique properties such as large band gap energy bowing [7] and the possibility of film growth lattice matched to Si, though, to the best of the author's knowledge, there is no published report on the successful growth of these materials on Si substrate to date. Due to the large energy gap bowing, the band gap energy of III-N-V alloys is expected to decrease with increasing nitrogen solid phase composition first, then go to a minimum value around mid-nitrogen composition, and finally increase up to the value for the corresponding group III nitride. The band gap reductions by the addition of nitrogen atoms in group III phosphides or arsenides has been experimentally verified in GaN_xP_{1-x} [8-10, 15, 16], GaN_xAs_{1-x} [17-19, 21, 23], InN_xP_{1-x} [28] and $Ga_xIn_{1-x}N_yAs_{1-y}$ [26] alloys in the low nitrogen composition range. The bowing was observed in

GaN-rich side of both GaN_xP_{1-x} [11] and GaN_xAs_{1-x} [22] as well.

The large band gap bowing in the III-N-V alloys can be explained by the large valence electron energy difference between nitrogen and other anions. It is well known in III-V compounds that the electrons in *s* and *p* orbitals contribute to the valence bond forming sp^3-hybridized state. Figure 1-1 shows average valence electron energy $(E_s+3E_p)/4$ of group III and group V elements in the sequence of the periodic

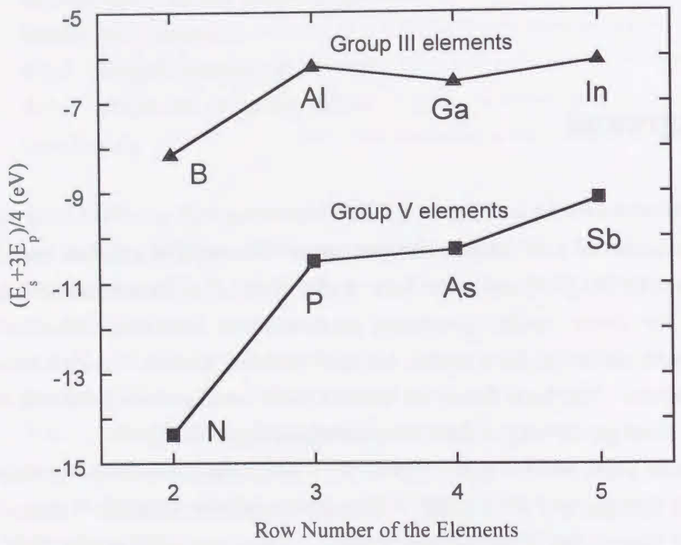

Figure 1-1. Average valence electron energy of group III and V elements. The lines are used only to guide the eye.

table, where the subscripts represent the corresponding orbits of the electron. The electron energy of the elements is taken from Herman and Skillman's value [29]. This average energy is referred to as "hybrid energy". The hybrid energy of the elements belonging to the rows 3 to 5 is very similar, and therefore, the valence band energy of the alloys made of (AlGaIn)(PAsSb) does not change significantly. However, this is

not the case for GaN_xP_{1-x}, for example, since there is a big jump in the energies between the second row and the third row of the periodic table for both group III and group V elements. This makes a large difference in the valence energy of the electron belonging to the Ga-P and Ga-N bond, and hence produces the large energy gap bowing. Due to the above mechanism, large band gap bowing is expected to exist in all alloys which include nitrogen and other group V elements as anions, and the same for alloys which include boron and other group III elements as cations (B-III-V alloys).

Some optical devices have been fabricated using III-N-V alloys. Employing $Ga_{0.7}In_{0.3}N_{0.01}As_{0.99}$-GaAs single quantum well as a active layer, continuous lasing operation with 1.3 μ m infrared (IR) emission was demonstrated at room temperature [30, 31]. Recently, red LEDs consisting of $GaN_{0.011}P_{0.989}$ p-n homojunction with the emission around 670 nm [32], and a $GaN_{0.029}As_{0.971}$ resonant-cavity avalanche photodiode operating at 1.064 μ m [33] have been demonstrated. However, the fundamental properties of these alloys are not well known yet. Both theoretical approaches and experimental investigations are ongoing for further understanding and applications of III-N-V alloys.

Among the III-N-V alloys, InN_xAs_{1-x} is expected to produce the narrowest band gap energy. There had been only one published report on the growth of InNAs [34] at the beginning of the present doctoral dissertation study.

1-2 Expectations for InN_xAs_{1-x} and the present research situation

Although it is not clear if the band gap energy bowing of III-N-V alloys is large enough to produce zero or negative band gap energy, these alloys can potentially produce a very narrow band gap energy. To produce such a narrow band gap, a nitrogen solid phase composition around the middle range is required. However it is very difficult to grow III-N-V alloys with such a high nitrogen composition because a large compositional miscibility gap [35, 36] is expected to exist due to the large difference in bond length between, for example, GaN (1.950Å) and GaP (2.360Å) in the case of GaN_xP_{1-x} alloys. The large difference in bond length is caused by the

electronic structure of the nitrogen atom, in which the valence electrons are strongly bound by its nucleus and hence located near the nucleus. On the other hand, the other group V atoms contain a large number of electrons and the valence electrons are not bound so strongly to its nucleus. These features can also be seen in Fig. 1-1. Due to the above mechanism, a large miscibility gap should exist in all the III-N-V alloys. Indeed, mid-nitrogen solid phase composition has not been achieved so far even in GaN_xP_{1-x} and GaN_xAs_{1-x} alloys which have been studied the most among all the III-N-V alloys.

Since InAs has a narrow band gap energy (0.36 eV [37] at room temperature) as compared to other group III arsenides or phosphides, the addition of only a small amount of nitrogen atoms into InAs may produce a very narrow band gap energy near 0 eV. It is very difficult to achieve such a narrow band gap with GaN_xP_{1-x}, GaN_xAs_{1-x} and InN_xP_{1-x} alloy systems because the band gap energies of GaP (2.26 eV [37]), GaAs (1.42 eV [37]) and InP (1.35 eV [37]) are too large. So, InN_xAs_{1-x} appears especially favorable for long wavelength device applications. From theoretical calculations, the band gap energy of InN_xAs_{1-x} is expected to range from 0 eV or even negative (around mid-nitrogen composition) to 1.89 eV for wurtzite InN [38-40]. Some of the calculated lines are shown in Fig. 1-2. The band gap energy of InN_xAs_{1-x} covers the red visible region of the light spectrum in InN-rich conditions. The negative band gap of InN_xAs_{1-x} around mid-nitrogen composition is further expected because of an experimental report of $InN_{0.38}As_{0.62}$ having a semi-metallic properties [38]. Though the calculations of the band gap energy of InN_xAs_{1-x} assumed InN to have wurtzite structure, InN also can exist in the meta-stable zincblende crystal phase structure [41-44]. If this is the case, the band gap energy of InN_xAs_{1-x} is expected to increase to 2.2 eV [45,46] for zincblend InN.

InN_xSb_{1-x} is another potential candidate for long wavelength device applications because InSb has a very narrow band gap energy of 0.17 eV [37] at room temperature. However InN_xSb_{1-x} is probably more difficult to grow than InN_xAs_{1-x} due to the larger difference in bond length between InN (2.140 Å) and InSb (2.810 Å) than the difference between InN (2.140 Å) and InAs (2.620 Å). To the best of the author's knowledge, there is no published report on InN_xSb_{1-x} growth to date.

The minimum band gap energy in conventional non-nitrogen containing III-V semiconductors can be achieved by $InAs_xSb_{1-x}$. $InAs_xSb_{1-x}$ was synthesized over the entire compositional range and shown to have a minimum band gap energy of about 0.10 eV with x around 0.35 [47, 48]. This means that conventional III-V semiconductors can not achieve light emission with wavelength longer than 12.4 μ m based on interband transitions. To break through this boundary using conventional

III-V compounds, a quantum cascade structure was proposed and is increasingly studied, though the device structure is very complicated [49-53]. Practically, the devices consisting of conventional III-V semiconductors are available for the wavelength range shorter than 5 μ m. For the longer wavelength applications, group IV-VI semiconductors such as $Sn_xPb_{1-x}Te$ (for a light emitter) and group II-VI semiconductors such as $Cd_xHg_{1-x}Te$ (for a photon detector) are currently used.

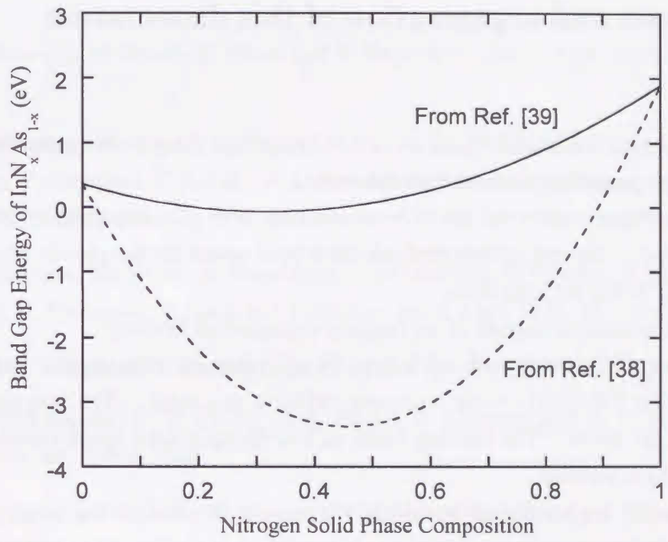

Figure 1-2. Estimated band gap energy of InN_xAs_{1-x}. The solid line was calculated by Yang et al. using the semi-empirical tight-binding method, and the dashed line by T. P. E. Broekaert et al. using a bowing coefficient of 18 eV experimentally obtained for GaN_xAs_{1-x} alloy in the low nitrogen composition range.

InN_xAs_{1-x} can potentially cover wavelengths longer than that of the yellow color of the light spectrum. This breaks through the boundary of conventional III-V semiconductors. InN_xAs_{1-x} is a promising material for IR application, and can be an alternative to all the conventional IR materials such as $Cd_xHg_{1-x}Te$, $Sn_xPb_{1-x}Te$,

$InAs_xSb_{1-x}$ and $Ga_xIn_{1-x}P_yAs_{1-y}$. Due to its narrow band gap, InN_xAs_{1-x} is interesting for low resistivity Ohmic contacts on III-V nitride devices as well. While many interesting points remain in the study of InN_xAs_{1-x}, only a few reports on the growth of InNAs have been published by the author and co-researchers [54-57], and by other groups [34, 38, 58, 59].

1-3 Purpose and organization of this dissertation

The objective of this doctoral study is to investigate the growth mechanism and the fundamental properties of a new material, InNAs.

The nitrogen source and the N/As source ratio both play important roles in the growth of InNAs. Several growth methods have been tested for the growth of InNAs over the course of this doctoral study.

This dissertation consists of six chapters organized as follows:

In chapter 2, the growth of InNAs by conventional metalorganic chemical vapor deposition (MOCVD) using ammonia (NH_3) is presented. The properties of grown InNAs are given. The limiting factor of low nitrogen solid phase composition of grown InNAs is verified.

In chapter 3, a plasma-assisted MOCVD process, in which all the mixed source gases are cracked by microwave excitation, is employed in an attempt to grow InNAs with higher nitrogen composition and good compositional uniformity. The results of the InN grown are also given.

In chapter 4, the growth of InNAs by molecular beam epitaxy (MBE) is presented. A successful growth of $InN_{0.38}As_{0.62}$ lattice matched to GaAs substrate by adjusting the growth conditions is demonstrated.

In chapter 5, plasma-cracked nitrogen and in situ plasma-generated arsine radicals are employed in an MOCVD system to achieve high N/As source flux ratio, with the goal of synthesizing InNAs with a high solid phase nitrogen composition. The key pathways for synthesis of InNAs single crystal film are discussed. The results of InAs grown using this MOCVD process are also presented.

Finally, chapter 6 concludes this work.

References

[1] S. Nakamura and G. Fasol: *The Blue Laser Diode*, 1st edition (Springer-Verlag, Heidelberg, 1997).

[2] S. Nakamura, T. Mukai and M. Senoh: Appl. Phys. Lett. **64**, (1994) 1687.

[3] S. Nakamura, M. Senoh, N. Iwasa and S. Nagahama: Appl. Phys. Lett. **67**, (1995) 1868.

[4] S. Nakamura, M. Senoh, N. Iwasa and S. Nagahama: Jpn. J. Appl. Phys. **34**, (1995) L797.

[5] S. Nakamura, M. Senoh, S. Nagahama, N. Iwasa, T. Yamada, T. Matsushita, H. Kiyoku, Y. Sugimoto, T. Kozaki, H. Umemoto, M. Sano and K. Chocho: Jpn. J. Appl. Phys. **37**, (1998) L627.

[6] S. Nakamura, M. Senoh, S. Nagahama, T. Matsushita, H. Kiyoku, Y. Sugimoto, T. Kozaki, H. Umemoto, M. Sano and T. Mukai: Jpn. J. Appl. Phys. **38**, (1999) L226.

[7] S. Sakai, Y. Ueta and Y. Terauchi: Jpn. J. Appl. Phys. **32**, (1993) 4413.

[8] J. N. Baillargeon, K. Y. Cheng, G. E. Hofler, P. J. Pearah and K. C. Hsieh: Appl. Phys. Lett. **60**, (1992) 2540.

[9] S. Miyoshi, H. Yaguchi, K. Onabe, R. Ito and Y. Shiraki: Appl. Phys. Lett. **63**, (1993) 3506.

[10] W. G. Bi and C. W. Tu: Appl. Phys. Lett. **69**, (1996) 3710.

[11] K. Iwata, H. Asahi, K. Asami and S. Gonda: J. Cryst. Growth **175/176**, (1997) 150.

[12] S. Miyoshi, H. Yaguchi, K. Onabe, Y. Shiraki and R. Ito: Jpn. J. Appl. Phys. **36**, (1997) 7110.

[13] H. Yaguchi, G. Biwa, S. Miyoshi, D. Aoki, K. Arimoto, K. Onabe, R. Ito and Y. Shiraki: J. Cryst. Growth **189/190**, (1998) 496.

[14] H. Yaguchi: J. Cryst. Growth **189/190**, (1998) 500.

[15] H. P. Xin, C. W. Tu, Y. Zhang and A. Mascarenhas: Appl. Phys. Lett. **76**, (2000) 1267.

[16] W. Shan, W. Walukiewicz, K. M. Yu, J. Wu, J. W. Ager III, E. E. Haller, H. P. Xin and C. W. Tu: Appl. Phys. Lett. **76**, (2000) 3251.

[17] M. Weyers and M. Sato: Appl. Phys. Lett. **62**, (1993) 1396.

[18] M. Sato: J. Cryst. Growth **145**, (1994) 99.

[19] W. G. Bi and C. W. Tu: Appl. Phys. Lett. **70**, (1997) 1608.

[20] K. Uesugi and I. Suemune: J. Cryst. Growth **189/190**, (1998) 490.

[21] S. Francoeur, G. Sivaraman, Y. Qiu, S. Nikishin and H. Temkin: Appl. Phys. Lett. **72**, (1998) 1857.

[22] K. Iwata, H. Asahi, K. Asami, R. Kuroiwa and S. Gonda: Jpn. J. Appl. Phys. **37**, (1998) 1436.

[23] W. K. Hung, M. Y. Chern, J. C. Fan, T. Y. Lin and Y. F. Chen: Appl. Phys. Lett. **74**, (1999) 3951.

[24] K. Uesugi, I. Suemune, T. Hasegawa, T. Akutagawa and T. Nakamura: Appl. Phys. Lett. **76**, (2000) 1285.

[25] P. J. Klar, H. Gruning, W. Heimbrodt, J. Koch, F. Hohnsdorf, W. Stolz, P. M. A. Vicente and J. Camassel: Appl. Phys. Lett. **76**, (2000) 3439.

[26] M. Kondow, K. Uomi, A. Niwa, T. Kitatani, S. Watahiki and Y. Yazawa: Jpn. J. Appl. Phys. **35**, (1996) 1273.

[27] T. Miyamoto and K. Iga: The Institute of Electronics, Information and Communication Engineers Vol. **83**, (2000) pp. 688-690 [in Jananese].

[28] W. G. Bi and C. W. Tu: J. Appl. Phys. **80**, (1996) 1934.

[29] F. Herman and S. Skillman: *Atomic Structure Calculations* (Prentice-Hall, New Jersey, 1963).

[30] M. Kondow, T. Kitatani, M. C. Larson, K. Nakahara, K. Uomi and H. Inoue: J. Cryst. Growth **188**, (1998) 255.

[31] K. Nakahara, M. Kondow, T. Kitatani, M. C. Larson and K. Uomi: IEEE Photon. Technol. Lett. **10**, (1998) 487.

[32] H. P. Xin, R. J. Welty and C. W. Tu: Appl. Phys. Lett. **77**, (2000) 1946.

[33] G. S. Kinsey, D. W. Gotthold, A. L. Holmes, Jr. and J. C. Campbell: Appl. Phys. Lett. **77**, (2000) 1543.

[34] S. V. Novicov, C. T. Foxon, T. S. Cheng, T. L. Tansley, J. W. Orton, D. E. Lacklison, D. Johnston, N. Baba-Ali, S. E. Hooper, L. C. Jenkins and L. Eaves: J. Cryst. Growth **146**, (1995) 340.

[35] G. B. Stringfellow: J. Cryst. Growth **27**, (1974) 21.

[36] G. B. Stringfellow: J. Cryst. Growth **58**, (1982) 194.

[37] See, for example, S. M. Sze: *Physics of Semiconductor Devices*, 2nd edition (John Wiley & Sons, New York, 1981) p. 849 (Appendix G).

[38] Y. C. Kao, T. P. E. Broekaert, H. Y. Liu, S. Tang, I. H. Ho and G. B. Stringfellow: Mater. Res. Soc. Symp. Proc. Vol. **423**, (1996) pp. 335-340, and the references therein.

[39] T. Yang, S. Nakajima and S. Sakai: Jpn. J. Appl. Phys. **36**, (1997) L320.

[40] N. Tit and M. W. C. Dharma-wardana: Appl. Phys. Lett. **76**, (2000) 3576.

[41] S. Strite, D. Chandrasekhar, David J. Smith, J. Sariel, H. Chen, N. Teraguchi and H. Morkoc: J. Cryst. Growth **127**, (1993) 204.

[42] D. Chandrasekhar, D. J. Smith, S. Strite, M. E. Lin and H. Morkoc: J. Cryst. Growth **152**, (1995) 135.

[43] A. Yamamoto, Y. Yamauchi, M. Ohkubo and A. Hashimoto: J. Cryst. Growth **174**, (1997) 641.

[44] A. Tabata, A. P. Lima, L. K. Teles, L. M. R. Scolfaro, J. R. Leite, V. Lemos, B. Schottker, T. Frey, D. Schikora and K. Lischka: Appl. Phys. Lett. **74**, (1999) 362.

[45] D. W. Jenkins, R. -D. Hong and J. D. Dow: Superlatt. Microstruc. **3**, (1987) 365.

[46] W. R. L. Lambrecht and B. Segall: Phys. Rev. **B43** (1991) 7070.

[47] A. G. Thompson and J. C. Woolley: Can. J. Phys. **45**, (1967) 255, and the references therein.

[48] M. Y. Yen, B. F. Levine, C. G. Bethea, K. K. Choi and A. Y. Cho: Appl. Phys. Lett. **50**, (1987) 927.

[49] J. Faist, F. Capasso, D. L. Sivco, C. Sirtori, A. L. Hutchinson and A. Y. Cho:

Science **264**, (1994) 553.

[50] R. Q. Yang, B. H. Yang, D. Zhang, C. -H. Lin, S. J. Murry, H. Wu and S. S. Pei: Appl. Phys. Lett. **71**, (1997) 2409.

[51] M. Rochat, J. Faist and M. Beck, U. Oesterle and M. llegems: Appl. Phys. Lett. **73**, (1998) 3724.

[52] A. Tredicucci, C. Gmachl, F. Capasso, D. L. Sivco, A. L. Hutchinson and A. Y. Cho: Appl. Phys. Lett. **74**, (1999) 638.

[53] A. Ishida and H. Fujiyasu: The Journal of The Institute of Electronics, Information and Communication Engineers Vol. **83**, (2000) pp. 376-382 [in Japanese].

[54] H.Naoi, Y. Naoi and S. Sakai: Solid State Electron. **41**, (1997) 319.

[55] S. Sakai, T. S. Cheng, T. C. Foxon, T. Sugahara, Y. Naoi and H. Naoi: J. Cryst. Growth **189/190**, (1998) 471.

[56] M. Hao, S. Sakai, T. Sugahara, T. S. Cheng and C. T. Foxon: J. Cryst. Growth **189/190**, (1998) 481.

[57] H. Naoi, D. M. Shaw, Y. Naoi, G. J. Collins and S. Sakai: J. Cryst. Growth (in press).

[58] M. Sopanen, H. P. Xin and C. W. Tu: Appl. Phys. Lett. **76**, (2000) 994.

[59] Y. -F. Chen, W. K. Hung, J. -C. Fan, J. S. Wang and H. H. Lin: Proc. Int. Workshop on Nitride Semiconductors (IWN 2000) IPAP Conf. Series **1**, pp. 437-440.

Chapter 2
Growth of InNAs by conventional MOCVD using NH_3

2-1 Introduction

For the growth of materials such as InNAs that have a large compositional miscibility gap, non-equilibrium growth methods such as metalorganic chemical vapor deposition (MOCVD) and molecular beam epitaxy (MBE) are favorable. As mentioned in chapter 1, there was only one published report on the growth of InNAs [1] at the beginning of the present doctoral study. The previous report covered the growth of GaN, InN, GaNAs and InNAs in an MBE system using a radio frequency (RF) plasma source of activated nitrogen. InNAs film was grown by unintentional arsenic incorporation from the background pressure in the MBE system into the depositing InN layer, which was revealed by Auger electron spectroscopy (AES) in-depth measurement. The detailed properties of the grown InNAs film such as crystal structure and nitrogen solid phase composition were not given. Thus, the present doctoral study was started using a conventional MOCVD for the growth of InNAs without any information on this new material.

In this chapter, the growth of InNAs by a conventional MOCVD using ammonia as the nitrogen source is presented [2]. The dependence of the nitrogen solid phase composition on the growth conditions is discussed. The reduction of band gap energy with increasing the nitrogen composition is demonstrated.

2-2 Growth apparatus and sample preparation

A schematic representation of the conventional MOCVD apparatus used herein is shown in Fig. 2-1. Arsine (AsH_3), ammonia (NH_3), trimethylindium (TMIn) and the hydrogen (H_2) carrier gas were all mixed about 30 cm upstream of the substrate.

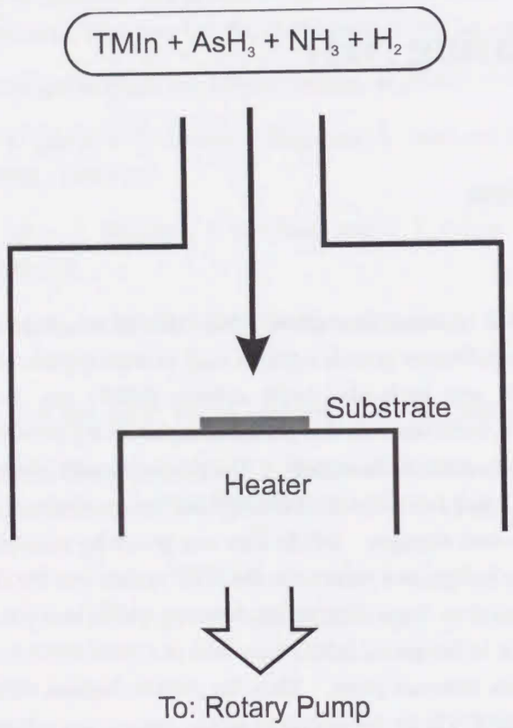

Figure 2-1. Schematic representation of the conventional MOCVD apparatus.

The substrate used in this experiment was n-type (100)GaAs. After cleavage into pieces about 1.0×1.5 cm^2, the substrates were degreased using organic solvents in an ultrasonic bath, followed by a base or acid solution etch and de-ionized water rinse, in order to remove any possible surface contaminants and native oxides from the substrate. After introduction into the growth chamber, before the deposition process the substrates were annealed in an ambient of arsine mixed with hydrogen at 900 ℃ for 5 minutes for the final surface preparation. The InNAs was grown directly on the prepared GaAs substrate without any pre-growth of GaAs or other buffer layers. The deposition process was initiated by simultaneous introduction of TMIn and NH_3 into the growth chamber. Upon completion of the deposition process, the TMIn flow to the growth chamber was stopped, while AsH_3 and NH_3 flow was continued until the substrate temperature fell below 400 ℃. The growth conditions of InNAs used in this experiment are summarized in table 2-1.

Table 2-1. Growth conditions.

Material	InNAs	InAs
Substrate	GaAs(100)	GaAs(100)
Growth Temperature	550-750℃	500℃
TMIn	0.01 sccm	0.22 sccm
AsH_3	5.0 sccm	20 sccm
NH_3	0.5-5 slm	0 slm
H_2(total)	1-4 slm	4 slm
Pressure	70 Torr	100 Torr
Growth Duration	120 minutes	30 minutes

The growth of InAs film was also performed for comparison of the properties to that of grown InNAs. Table 2-1 gives the InAs growth conditions as well.

The grown layers were characterized by scanning electron microscopy (SEM), x-ray diffraction (XRD) and Fourier transformation infrared spectroscopy (FTIR).

2-3 Results and discussion

2-3-1 Surface morphology of the grown layer

All the InNAs layers were island grown, and no continuous film was obtained except for InAs. A surface micrograph and cross-sectional view of the typical InNAs sample is shown in Fig. 2-2(a) and (b), respectively. The island shape is rectangular along the <011> direction, which indicates that the grown layer has cubic symmetry. The density of the grown islands (the number of islands per unit area) decreased with the increase in the growth temperature and NH_3 flow rate. The volume of each island increased with the increase in the growth temperature while it hardly changed by varying NH_3 flow rate. The surface coverage, c (the area covered by the grown layer), is in the range of 0.28-0.70, depending on the solid composition and the growth conditions. There was no systematic relationship between the coverage, c and the growth temperature, while the coverage decreased with increasing NH_3 flow rate. It can be seen in Fig 2-2(b) that each island is facetted by {111} plane, which is verified by the angle of 54.7° between <011> and the facet. This was true for all the other InNAs samples.

The surface of InAs film appeared mirror-like to the naked eye. The thickness of the InAs film was 1.3 μ m. The surface micrograph of the InAs sample is given in Fig. 2-2(c).

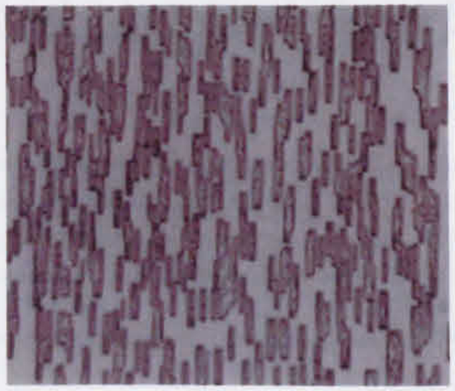

Figure 2-2(a). Surface micrograph of $InN_{0.034}As_{0.966}$ sample.

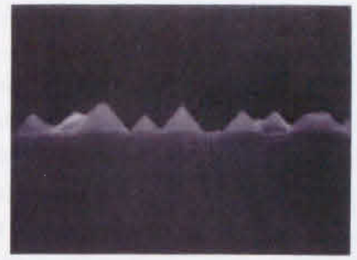

Figure 2-2(b). Cross-sectional view of $InN_{0.034}As_{0.966}$ sample.

Figure 2-2(c). Surface micrograph of InAs sample.

2-3-2 XRD pattern and absorption coefficient of grown InNAs

The crystallinity of the grown layers was investigated by a θ-2θ mode XRD with a powder diffractometer using the radiation of Cu Kα_1 and Kα_2. The XRD measurement was performed over the 2θ range of 20-80° for all the samples, and two peaks from (200) and (400)InNAs were observed along with the expected (200) and (400)GaAs diffraction peaks from the GaAs substrate. No other peak was observed in those diffraction profiles. Fig. 2-3(a) shows θ-2θ mode XRD patterns of samples near the GaAs(200) diffraction peak. The peaks around 29.5° and 31.6° are from zincblende InNAs(200) and GaAs(200), respectively. The nitrogen solid phase composition of InNAs in each sample was estimated, assuming Vegard's law, by the lattice constant calculated from the XRD peak position without taking account of any possible effects of lattice strain. The nitrogen solid phase compositions of these samples were determined to be 0.014, 0.019 and 0.034 as shown in the figure.

Fig. 2-3(b) shows the squared absorption coefficient, α^2, vs. photon energy calculated from transmission spectra of the same samples. The transmission spectra of the samples were measured by FTIR at room temperature using a clean GaAs substrate as a reference. In calculating the absorption coefficient, α, the coverage, c, of each sample is measured and taken into account. Light scattering by the island edge can be accommodated by adjusting the 100% transmission level. The α^2 vs. photon energy plot in Fig. 2-3(b) is almost linear indicating that the InNAs ternary alloys obtained have a direct band gap. The difference in the gradient in these plots is mainly caused by the inaccuracy in determining the surface coverage, c. This inaccuracy also produces an error in determining band gap energy, which is indicated by the error bar in Fig. 2-6. The divergence from straight lines at lower energy seems to be influenced by the inhomogeneity of composition and the crystal imperfections. The results shown in Fig. 2-3 demonstrate that the band gap of InNAs actually becomes narrower with increase in the nitrogen solid phase composition, as predicted [3-6].

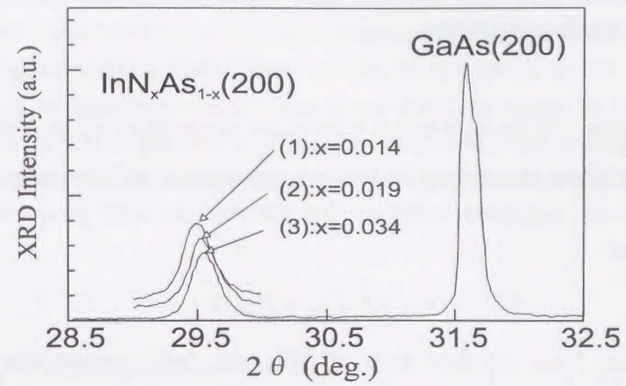

(a) Shift in XRD peak position

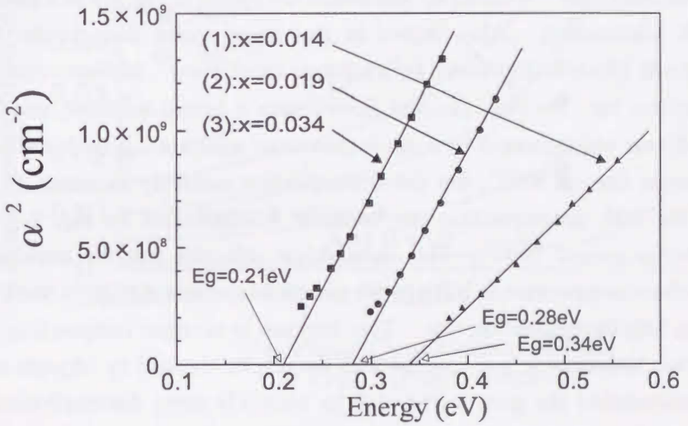

(b) Shift in band gap energy

Figure 2-3. XRD profiles and band gap energy: (a) XRD; (b) plots of absorption coefficient squared versus photon energy.

2-3-3 Dependence of the nitrogen solid phase composition on the growth conditions

Figure 2-4 shows nitrogen solid phase composition X_N^S as a function of the nitrogen gas phase composition for InNAs layers grown at different temperatures. The solid lines are calculated assuming that the nitrogen solid phase composition is expressed as

$$X_N^S = k \cdot F_{NH_3} / (k \cdot F_{NH_3} + F_{AsH_3}), \qquad (1)$$

where F_{NH3}, F_{AsH3} are flow rates of NH_3 and AsH_3, respectively, and k is a decomposition rate constant of NH_3. The experimental nitrogen solid composition increases with increasing NH_3 gas phase composition and growth temperature. The decomposition rate constant of NH_3, k, can be determined by fitting experimental points to the calculated solid lines. k values so determined are shown in Fig. 2-5 as a function of the growth temperature. Also shown in the figure (solid line) is the NH_3 decomposition rate which is determined by a separate experiment. In determining the NH_3 decomposition rate, the NH_3 gas was flowed over a heated substrate, and NH_3 content downstream was measured by a quadrupole mass analyzer. NH_3 decomposes at temperatures as low as 500℃, but the decomposition suddenly increases around 760-800℃. The NH_3 decomposition rate constant, k, determined by Fig. 2-4 also suddenly increases around 760℃. This coincidence indicates that the increase of nitrogen solid phase composition in InNAs with growth temperature is simply due to the increase of the NH_3 decomposition rate. This increase in nitrogen composition with increasing growth temperature is in contrast with the results obtained by Miyoshi et al. [7]. They demonstrated the growth of GaNP by MOCVD using dimethylhydrazine (DMHy) as the nitrogen source at the growth temperature around 650℃. In their report, the nitrogen composition in GaNP decreased with increasing growth temperature. Later on, they verified that the decrease in the nitrogen composition was caused by increasing nitrogen desorption from the film surface during growth at higher temperatures, by applying a growth interruption technique [8]. The resultant vacant sites are expected to be occupied by the phosphorous atoms. The different behaviors of nitrogen solid phase composition is probably due to the different properties of the nitrogen sources. DMHy is much easier to decompose than NH_3. It decomposes almost completely at a temperature higher than 550℃ [9] and hence their growth condition is expected to be equivalent to that of MOCVD using nitrogen-related radical species. Indeed, a very similar effect was observed in GaNAs growth by low-pressure

MOCVD using plasma-cracked NH_3 [10]. This effect was also observed in MBE growth of GaNP [11] and InNP [12] using a radio frequency activated nitrogen radical beam. The nitrogen desorption should have occurred in the InNAs growth herein. However, NH_3 can be completely decomposed above 900℃ as shown in Fig. 2-5. The increase in the growth temperature is expected to enhance the NH_3 decomposition much more significantly than the nitrogen desorption leading to the increase in nitrogen content.

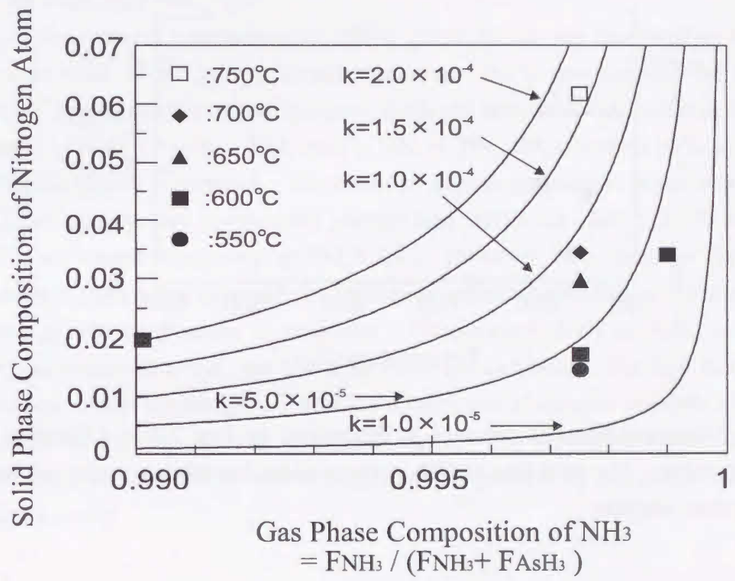

Figure 2-4. Dependence of nitrogen solid phase composition on gas phase composition. The solid lines are calculated assuming that the nitrogen solid phase composition is expressed as equation (1).

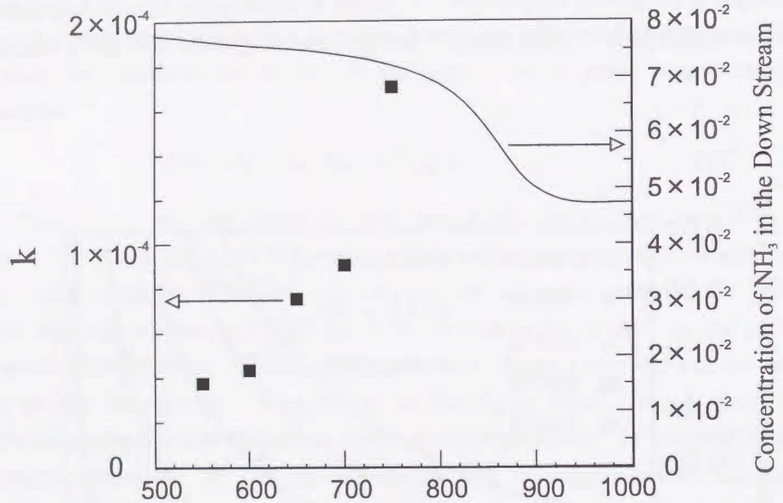

Figure 2-5. Decomposition rate constant, *k*, determined by Fig. 2-4 as a function of growth temperature. The solid line is NH_3 concentration downstream measured by a quadrupole mass analyzer.

Miyoshi et al. also reported on the increase of nitrogen composition in GaNP with increasing TMGa flow rate, i.e., the growth rate [7]. This phenomenon was explained by surface coverage by the next growing layer before the nitrogen desorption, i. e., the "freezing out" of the surface layer before the occurrence of the nitrogen desorption [8]. Herein, the InNAs growth rate also increased with increasing TMIn flow rate from 0.01 sccm up to 0.02 sccm at the growth temperature of 600℃ and NH_3 flow rate of 2000 sccm. However, the increase in the growth rate resulted in a decrease in the nitrogen content from 1.7% to 0.4% and the resultant band gap energy increased from around 0.26eV to 0.31eV. This can be also explained by the insufficient NH_3 decomposition. Even if the effective nitrogen source supply is low,

the nitrogen incorporation should be enhanced with increasing the growth rate by the "freezing out" effect. However, under a low effective nitrogen source supply, the number of nitrogen atoms that can be incorporated per unit growing volume should decrease with an increase in the growth rate. This effect is expected to affect much more strongly than the "freezing out" effect, resulting in the reduction of nitrogen content in the InNAs. The $InN_{0.004}As_{0.996}$ sample was also island grown with the surface coverage, *c*, larger than 0.95.

The further increase in TMIn flow above 0.02 sccm or the further decrease in the growth temperature below 500℃ resulted in only InAs phase growth, even when the N/As source ratio was 100.

The nitrogen composition of InNAs grown herein was increased up to 6.1%. Further increase of the growth temperature above 750℃ may increase the nitrogen content of InNAs, but the surface becomes rough and it is impossible to obtain a smooth surface. In order to grow a high quality InNAs film with a smooth surface, a lower growth temperature is required. The optimum growth temperature is probably around 500℃ because the two components constructing InNAs i.e., InN [13-19] and InAs [20-22], are commonly grown around 500℃. However, NH_3 does not decompose efficiently at such a low temperature. Hence, an alternate nitrogen source available at the low growth temperature is necessary. Plasma-cracked N_2 or NH_3, as well as DMHy as discussed above, are the most obvious candidates. The low temperature growth has another advantage, which is the suppression of nitrogen desorption from the surface of the growing layer as mentioned above. The growth of InNAs films with high nitrogen composition as well as high quality is possible by using these alternative nitrogen sources.

2-3-4 Nitrogen solid phase composition and band gap energy

Figure 2-6 shows band gap energy vs. nitrogen solid phase composition for all the samples. The lines are calculated values [4, 5]. The error bars in the experimental data were caused by the inaccuracy of surface coverage, *c*, measurement as mentioned in sub-section 2-3-2. The band gap energy decreases with increase in the nitrogen content as predicted [3-6]. The maximum nitrogen composition obtained in this experiment is 6.1%, and this sample exhibits the minimum band gap energy around 0.12 eV (the value at the middle of the error bar) among all the samples. This value is comparable to the minimum band gap energy in conventional III-V semiconductors i.e., 0.10 eV achieved by $InAs_xSb_{1-x}$ material system [23, 24]. It is noteworthy that only

6.1% of nitrogen incorporated into InAs produced such a narrow band gap energy. A little further increase in the nitrogen composition is likely to record a new minimum band gap energy among all the III-V semiconductors. The experimental data are so far in good agreement with the result calculated by Yang et al. [5], with the semi-empirical tight-binding method.

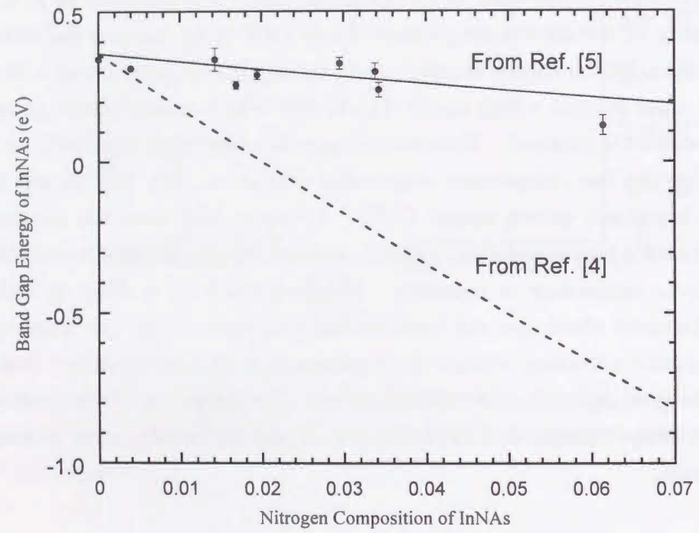

Figure 2-6. Band gap energy of InN_xAs_{1-x} as a function of nitrogen solid phase composition, x. The solid line was calculated by Yang et al. using the semi-empirical tight-binding method, and the dashed line by T. P. E. Broekaert et al. using a bowing coefficient of 18 eV experimentally obtained for GaN_xAs_{1-x} alloy in the low nitrogen composition range.

2-4 Conclusions

A conventional MOCVD system using NH_3 as the nitrogen source was employed for the growth of InNAs. InN_xAs_{1-x} (x = 0∼0.061) was obtained. All the deposited InNAs layers were island grown and had the direct transition band structure. The increase in growth temperature raised the nitrogen solid phase composition, explained by the increased NH_3 decomposition rate at higher temperature. The increase in the gas phase composition of NH_3 also raised the nitrogen solid phase composition. The growth rate was varied by changing TMIn flow rate, and the nitrogen solid phase composition decreased with increase in the growth rate. The band gap energy decreased with increasing nitrogen solid phase composition, and the minimum band gap energy of 0.12 eV was obtained for $InN_{0.061}As_{0.939}$. This energy value is comparable to the minimum band gap of 0.10 eV achieved by $InAs_xSb_{1-x}$ material system among all the conventional III-V semiconductors. It is noteworthy that only 6.1% of nitrogen into InAs produced such a narrow band gap.

Since NH_3 decomposes efficiently above 900℃, the necessity to use DMHy or plasma-cracked N_2 or NH_3 as the nitrogen source was suggested for the growth of good quality InNAs film with higher nitrogen composition.

References

[1] S. V. Novicov, C. T. Foxon, T. S. Cheng, T. L. Tansley, J. W. Orton, D. E. Lacklison, D. Johnston, N. Baba-Ali, S. E. Hooper, L. C. Jenkins and L. Eaves: J. Cryst. Growth **146**, (1995) 340.

[2] H.Naoi, Y. Naoi and S. Sakai: Solid State Electron. **41**, (1997) 319.

[3] S. Sakai, Y. Ueta and Y. Terauchi: Jpn. J. Appl. Phys. **32**, (1993) 4413.

[4] Y. C. Kao, T. P. E. Broekaert, H. Y. Liu, S. Tang, I. H. Ho and G. B. Stringfellow: Mater. Res. Soc. Symp. Proc. Vol. **423**, (1996) pp. 335-340, and the references therein.

[5] T. Yang, S. Nakajima and S. Sakai: Jpn. J. Appl. Phys. **36**, (1997) L320.

[6] N. Tit and M. W. C. Dharma-wardana: Appl. Phys. Lett. **76**, (2000) 3576.

[7] S. Miyoshi, H. Yaguchi, K. Onabe, R. Ito and Y. Shiraki: Appl. Phys. Lett. **63**, (1993) 3506.

[8] S. Miyoshi, H. Yaguchi, K. Onabe, Y. Shiraki and R. Ito: Jpn. J. Appl. Phys. **36**, (1997) 7110.

[9] Presented in: S. Sugiyama, T. Shimizu, Y. Kojima, T. Miyata, S. Takata and M. Ishii: Ext. Abstr. (The 54th Autumn Meet., 1993); The Japan Society of Applied Physics, No.1, p. 324 (30p-ZS-6) [in Japanese].

[10] M. Weyers and M. Sato: Appl. Phys. Lett. **62**, (1993) 1396.

[11] W. G. Bi and C. W. Tu: Appl. Phys. Lett. **69**, (1996) 3710.

[12] W. G. Bi and C. W. Tu: J. Appl. Phys. **80**, (1996) 1934.

[13] A. Wakahara, T. Tsuchiya and A. Yoshida: Vacuum **41**, (1990) 1071.

[14] A. Wakahara and A. Yoshida: Appl. Phys. Lett. **54**, (1989) 709.

[15] Q. Guo, H. Ogawa, H. Yamamoto and A. Yoshida: Appl. Phys. Lett. **66**, (1995) 715.

[16] S. Strite, D. Chandrasekhar, David J. Smith, J. Sariel, H. Chen, N. Teraguchi and H.

Morkoc: J. Cryst. Growth **127**, (1993) 204.

[17] D. Chandrasekhar, D. J. Smith, S. Strite, M. E. Lin and H. Morkoc: J. Cryst. Growth **152**, (1995) 135.

[18] A. Yamamoto, Y. Yamauchi, M. Ohkubo and A. Hashimoto: J. Cryst. Growth **174**, (1997) 641.

[19] A. Tabata, A. P. Lima, L. K. Teles, L. M. R. Scolfaro, J. R. Leite, V. Lemos, B. Schottker, T. Frey, D. Schikora and K. Lischka: Appl. Phys. Lett. **74**, (1999) 362.

[20] S. K. Haywood, R. W. Martin, N. J. Mason and P. J. Walker: J. Electron. Mater. **19**, (1990) 783.

[21] K. Y. Ma, Z. M. Fang, R. M. Cohen and G. B. Stringfellow: J. Electron. Mater. **21**, (1992) 143.

[22] C. H. Chen, G. B. Stringfellow and R. W. Gedridge, Jr.: J. Cryst. Growth **126**, (1993) 309.

[23] A. G. Thompson and J. C. Woolley: Can. J. Phys. **45**, (1967) 255, and the references therein.

[24] M. Y. Yen, B. F. Levine, C. G. Bethea, K. K. Choi and A. Y. Cho: Appl. Phys. Lett. **50**, (1987) 927.

Chapter 3
Attempt at InNAs growth by plasma-assisted MOCVD

3-1 Introduction

The nitrogen composition of InNAs could not be increased above 6.1% by conventional metalorganic chemical vapor deposition (MOCVD) due to insufficient NH_3 decomposition. It was concluded in chapter 2 that a nitrogen source useful in the temperature range for InNAs growth (around 500℃) is necessary in order to obtain high quality InNAs film with higher nitrogen solid phase composition. Dimethylhydrazine (DMHy) and plasma-cracked N_2 or NH_3 are the most promising candidates as the alternative nitrogen sources. Since there was no extra port available for the attachment of DMHy in the MOCVD system, it was decided to adopt the latter choice. N_2 was employed rather than NH_3 simply because two nitrogen radicals can be obtained from the one molecule. The conventional MOCVD growth chamber presented in chapter 1 was slightly modified for the addition of plasma generation. Commonly, N_2 is cracked by the generation of a remote nitrogen plasma and then introduced into the downstream MOCVD growth chamber [1-5]. In the present MOCVD system, all the mixed source molecules are cracked simultaneously, due to the difficulty of system modification for separate N_2 plasma generation. In fact, it was speculated that the simultaneous cracking of all the source molecules might be better for the growth of InNAs film with good compositional uniformity.

In this chapter, plasma-assisted MOCVD of InNAs is presented. All the mixed source gases are cracked upstream of the growth substrate by microwave

excitation. After the explanation of growth apparatus, the growth of InN is given first [6], and then the addition of AsH_3 into the plasma stream for the growth of InNAs is demonstrated [7].

3-2 Growth apparatus

A diagram of the plasma-assisted MOCVD growth apparatus used in this experiment is shown in Fig. 3-1. The mixture of TMIn, N_2, AsH_3 and the H_2 carrier gas was decomposed inside a quartz tube by microwave excitation for the growth of InNAs. In the case of InN growth, AsH_3 flow was set to zero during the deposition process. The plasma column was about 20 cm long along the gas stream. The distance between the bulk plasma and the growth substrate was about 15 cm. The substrate used in this experiment was n-type (100)GaAs.

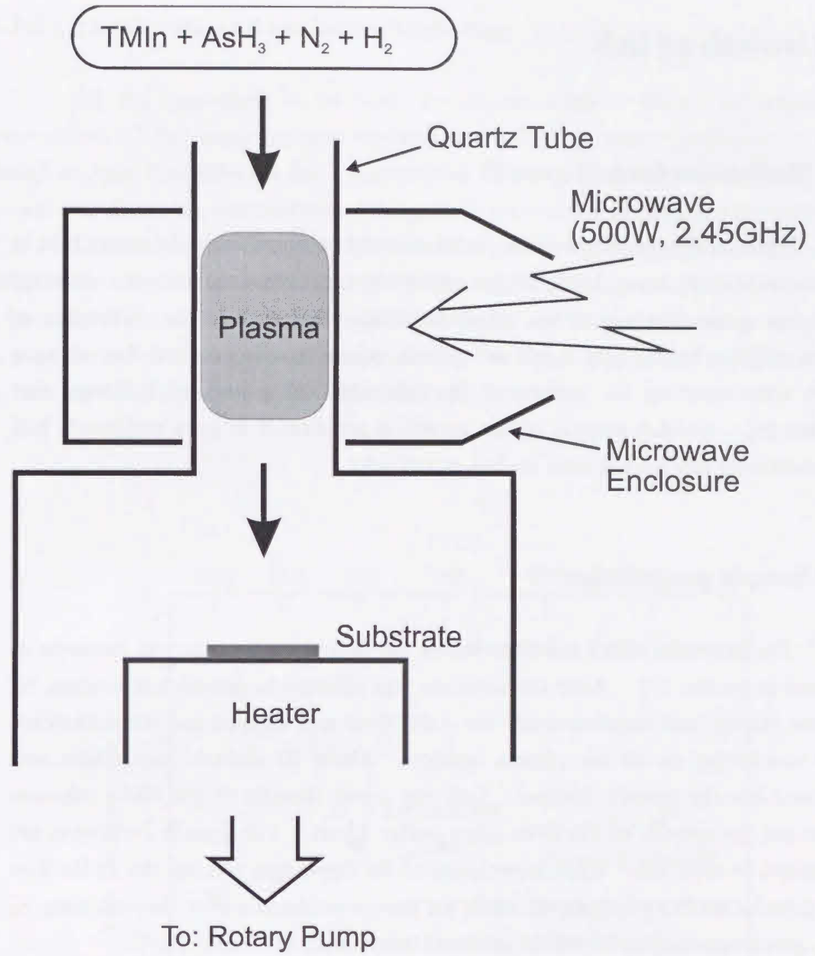

Figure 3-1. Diagram of the plasma-assisted MOCVD growth apparatus.

3-3 Growth of InN

3-3-1 Motivation for InN growth

Since all the mixed gases are simultaneously decomposed in the quartz tube in this growth system, many kinds of gas phase chemical reactions between activated species can occur upstream of the substrate, which may result in the elimination of nitrogen radicals before they reach the growth substrate. To confirm that nitrogen radicals were reaching the surface of the substrate, the growth of InN was first attempted [6]. Another purpose of this growth experiment is to grow zincblende InN since zincblende InN has not been studied extensively.

3-3-2 Sample preparation

The treatment of the substrate before the deposition process was the same as discussed in section 2-2. After the substrate was adjusted to growth temperature, N_2 flow was started, and simultaneously the AsH_3 flow was stopped and the microwave power was turned on for the plasma ignition. About 10 seconds later, TMIn was introduced into the growth chamber. InN was grown directly on the GaAs substrate without any pre-growth of GaAs or other buffer layers. The growth conditions are summarized in table 3-1. Upon completion of the deposition process, the TMIn flow to the growth chamber was stopped, while the plasma production from the remaining N_2 and H_2 gases was continued until the substrate temperature fell below 300℃.

The grown layers were characterized by x-ray diffraction (XRD).

Table 3-1. Growth conditions for InN.

Substrate	GaAs(100)
Growth Temperature	350-600℃
TMIn	0.02 sccm
AsH_3	0 sccm
N_2	250 sccm
H_2(total)	420 sccm
Pressure	3 Torr
Microwave Power	500 W (2.45GHz)
Growth Duration	180 minutes

3-3-3 Growth rate and surface morphology

All the deposited layers were continuous films. X-ray photoelectron spectroscopy (XPS) measurements revealed that the films were composed of InN though oxygen was detected [8]. Carbon was almost removed after etching. The growth rate decreases with increasing the growth temperature at the activation energy, E_a = 3.4 kcal/mol as shown in Fig. 3-2, when the growth rate is expressed as $g_o exp(E_a/kT)$. In this figure, the vertical axis is the film thickness. Since the growth duration is the same (180 min.) for all the samples, this figure also shows a relative growth rate as a function of reciprocal growth temperature. The film thickness data in Fig. 3-2 will be used for the comparison to the XRD data in Fig. 3-5 later.

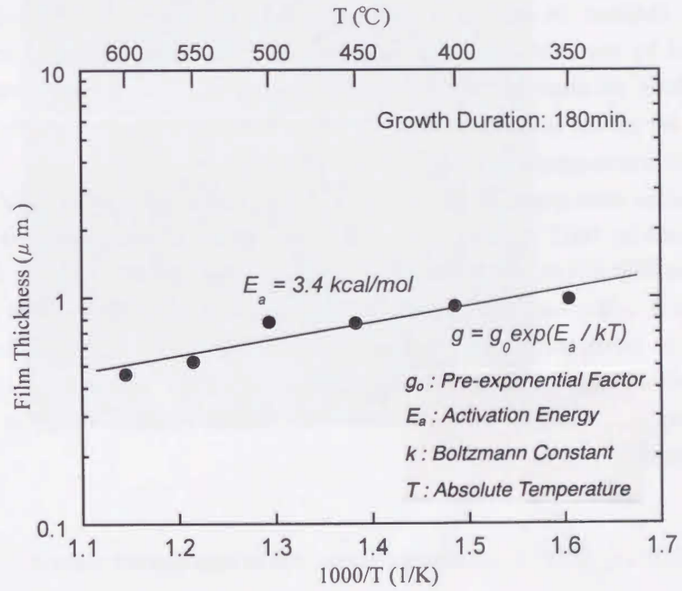

Figure 3-2. Film thickness (or growth rate) of InN.

The decrease in the growth rate with increase in the growth temperature is reasonable. InN begins to decompose around 550℃ even under the atmospheric pressure [9]. The reduced pressure employed in this InN growth experiment is 3 Torr, which is much lower than the atmospheric pressure, and the decomposition of InN is expected to occur in all the growth temperature range used. The enhancement of InN decomposition at higher temperature was revealed by the increase in InN vapor pressure with increasing the temperature with an activation energy of 69 kcal/mol [10,11]. Consequently, it should be concluded that the growth of InN was competing with InN decomposition. TMIn is expected to be completely decomposed in the plasma stream by collisions with electrons, plasma-generated H-radicals and N-radicals. If this is the case, the heat from the growth substrate is not used for TMIn decomposition i.e., raising the temperature never increases the growth rate. Hence, the increase in the growth temperature increased only the InN decomposition rate, leading to the reduced growth rate at higher temperature. This reduction of growth rate is in contrast with Sato's result [5] obtained by plasma-assisted MOCVD in which N_2 was separately decomposed by microwave excitation and triethylindium (TEIn) was used as the In source without pre-cracking. In Sato's report, the InN growth rate increased with increasing the growth temperature from 400℃ to 600℃, which can be explained by enhanced TEIn decomposition at higher temperature.

Surface micrographs are shown in Fig. 3-3 for the samples grown at (a) 500℃, (b) 550℃ and (c) 600℃. The surface of the samples grown below 500℃ is smooth as shown in Fig. 3-3(a), and appeared mirror-like to the naked eye. The dust-like particle in Fig. 3-3(a) was used in order to focus on the surface. The surface color of these samples grown below 500℃ was gold, though the GaAs substrate surface color had some effect on the film color because the films were thin. The real color of these grown layers was expected to be amber. The surface becomes rough at growth temperatures above 550℃.

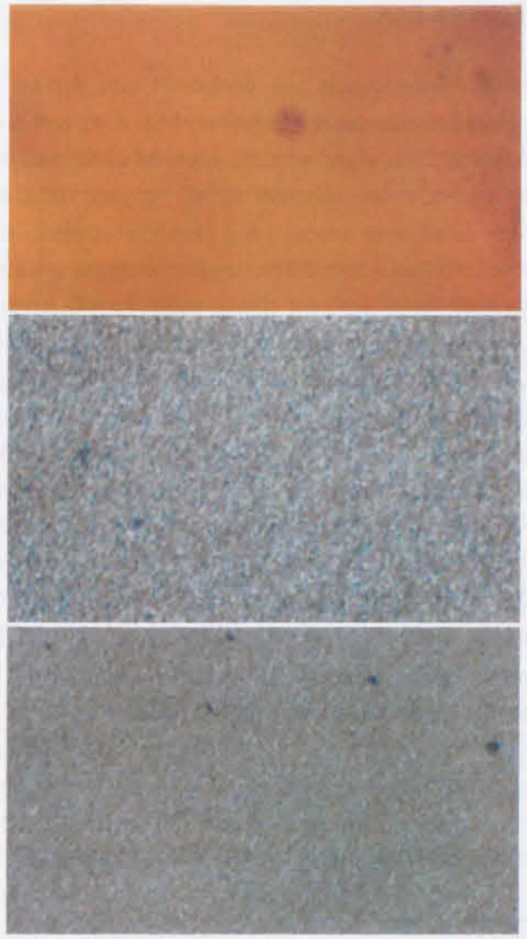

Figure 3-3. Surface micrographs of InN samples grown at (a) 500℃, (b) 550℃ and (c) 600℃.

3-3-4 Crystallinity of grown InN

A θ-2θ mode XRD measurement was performed over the 2θ range of 20-80° using a powder diffractometer and the radiation of Cu $K\alpha_1$ and $K\alpha_2$. The diffractions from zincblende InN(200) along with the expected (200) and (400)GaAs diffraction peaks from the substrate were observed for all samples. The diffraction peak from InN(400) was very small, even unobservable for some samples. Figure 3-4 shows the XRD profile around the GaAs(200) diffraction for the sample grown at 450℃. The shape of the InN(200) peak varies with the change in the growth temperature as shown in Fig. 3-5. As the growth temperature increases from 450℃ to 550℃, the XRD intensity decreases, while the full width at half maximum (FWHM) stays at constant. This is explained by the reduction of the film thickness at higher growth temperatures as shown in Fig. 3-2. When the growth temperature decreases from 450℃, the film thickness increases. However the XRD intensity decreases. This means the deterioration of the film quality, which can also be seen in the sudden increase in the **FWHM** of XRD below growth temperature of 450℃. The crystallinity of the film grown at 600℃ seems better than other samples because the FWHM of XRD is relatively low and the intensity is higher than other samples though the film is the thinnest. However the surface is rough as shown in Fig. 3-3. The best temperature in this InN growth experiment seems to be 450-500℃

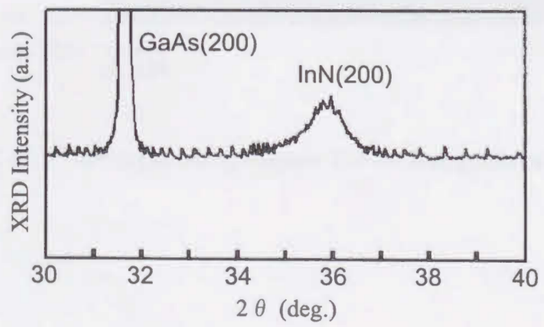

Figure 3-4. XRD from InN grown at 450℃.

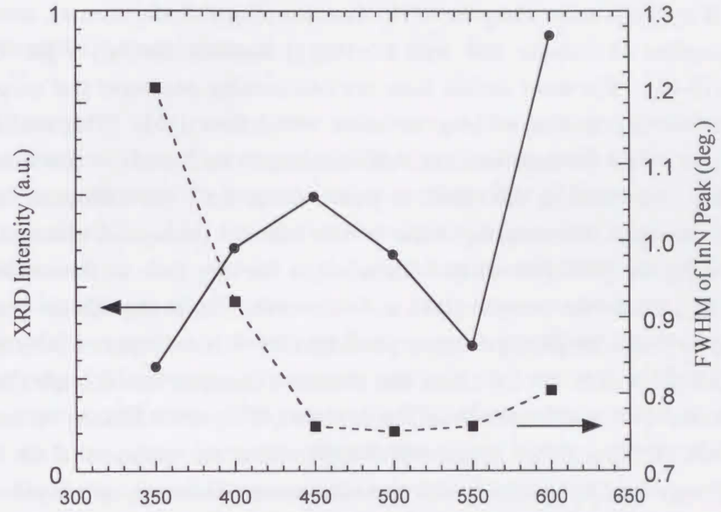

Figure 3-5. XRD intensity and FWHM of the InN peak. The lines are used only to guide the eye.

The XRD intensities from InN(200) are more than ten times weaker than that of GaAs(200), i.e., too weak for the given thickness of InN, which means the crystal imperfections are present in the film. The mixture of wurtzite InN in the grown layers was speculated to be the cause of the imperfections. The growth of the InN is very unstable. It is known that even if the zincblende InN is oriented epitaxially to the GaAs, stacking faults occur along the <111> direction of zincblende structure, resulting in the formation of wurtzite InN with the [0001] direction parallel to the <111> direction [12-14]. For more details, there are two stacking sequences that make the plane perpendicular to the stacking direction the densest [15]. The zincblende (face-centered cubic) structure has ABCABC stacking along the <111> direction. If the stacking is ordered in ABABAB sequence along the <111> direction of the zincblende structure, the stacking order is the wurtzite (hexagonal close-packed) structure along the [0001] direction. Therefore, a stacking fault in the zincblende structure can generate the wurtzite phase and vice versa. Supposing that the wurtzite InN was grown with the [0001] direction parallel to the <111> direction of zincblende symmetry, XRD ω-2θ (θ-2θ) scan was measured changing the tilt angle (Psi) of the sample to detect a diffraction from the wurtzite ($10\bar{1}0$) or ($01\bar{1}0$)InN, by another XRD system (Philips, X'Pert, Type: PW3040/00) using the radiation of Cu Kα_1 coming through Ge(220) quadru-crystal monochromator. However, no wurtzite peak was observed (The position of the wurtzite InN peak is: Psi~$\pm$35.26°, 2θ~29.05°, when one of the <011> direction of the GaAs substrate is parallel to the incident x-ray plane.). Morkoc's group investigated the stacking sequence in InN grown on (100)GaAs by MBE with electron cyclotron resonance (ECR) nitrogen plasma source, using high-resolution transmission electron microscopy (HR-TEM). They reported that some regions contained both domains, while some regions were heavily faulted and had no long range stacking order and it was impossible to assign either phase [12, 13]. If this is the case for all regions of the grown InN, the grown layer may be considered amorphous. The InN obtained in this growth experiment was probably almost amorphous with the zincblende phase in a slight majority, resulting in the small and broad XRD peak from InN(200).

A photoluminescence (PL) measurement was performed on these InN samples at room temperature and 20K, using an Ar-ion laser operating at 488 nm as the excitation source. However, no emission associated with wurtzite or zincblende InN was observed.

3-4 Addition of AsH_3 into plasma stream for the growth of InNAs

3-4-1 Sample preparation

Though of poor quality, InN was grown in this plasma-assisted MOCVD system. AsH_3 was then added into the plasma stream for the growth of InNAs [7].

The treatment of the substrate before the deposition process was the same as shown in section 2-2. After the substrate was adjusted to growth temperature, N_2 flow was started and the flow rate of AsH_3 was adjusted, and finally the TMIn was introduced into the growth chamber as soon as the microwave power was turned on. The deposition was performed directly on the GaAs substrate without any pre-growth of GaAs or other buffer layers. The growth conditions are summarized in table 3-2. Upon completion of the deposition process, the TMIn flow to the growth chamber was stopped, while the plasma production from the remaining N_2, H_2 and AsH_3 gases was continued until the substrate temperature fell below 300℃.

The grown layers were characterized by x-ray diffraction (XRD).

Table 3-2. Growth conditions for InNAs.

Substrate	GaAs(100)
Growth Temperature	450, 500℃
TMIn	0.02 sccm
AsH_3	0.067-5.0 sccm
N_2	250 sccm
H_2(total)	420 sccm
Pressure	3 Torr
Microwave Power	500 W (2.45GHz)
Growth Duration	125-180 minutes

3-4-2 Surface morphology and crystallinity of deposited layer

A θ-2θ mode XRD measurement was performed in the same way as for the InN samples. The variations of XRD profiles with the group V source flow ratio of AsH_3/N_2 are shown in Fig. 3-6(a), (b) for the samples grown at 450℃, 500℃ respectively. The XRD profile of the InN sample grown at 450℃ in Fig. 3-4 is reprinted in Fig. 3-6(a), and the profile of another InN sample grown at 500℃ is given in Fig. 3-6(b) for a systematic comparison of the XRD data. Though the profiles are plotted in the 2θ range just around the GaAs(200) diffraction, no diffraction peak except for (200), (400)InAs and (200), (400)InN and the expected (200), (400)GaAs was observed. The growth duration of each sample is given in these figures. As is seen in the figures, no crystallized InNAs was obtained by this plasma-assisted MOCVD process. The diffraction peaks from InAs(200) can be seen in the samples grown at lower AsH_3/N_2 ratios, where the diffraction from InAs(400) was also observed. The surface micrographs of these samples are shown in Fig. 3-7(a) and (b) respectively. In these pictures, many dust-like particles can be seen. During the deposition process, black film deposited on the inside wall of the growth chamber both just upstream and downstream of the bulk plasma. This film deposition partly covered the inside wall of the bulk plasma region and it sometimes flaked off. In the case of InN growth, black-brown film deposited just upstream and downstream of the bulk plasma without any deposition in the bulk plasma region, and the dust-like particles were hardly seen on the sample surface. Those black particles in the picture probably came from As-related materials that fell from the wall onto the growth substrate. There was almost no film deposition on the substrate for the TG3566 sample processed at the highest AsH_3/N_2 ratio, for which the volume of the deposition on the inside wall just down stream of the bulk plasma was the largest. The thickness of the film on the substrate increased with decreasing AsH_3/N_2 source ratio and was about 0.5 μm for the samples of TG3572 and TG3571, while the volume of the deposition on the inside wall just downstream of the bulk plasma decreased and the deposition in the bulk plasma region became less with decreasing AsH_3/N_2 ratio. The film growth rates of TG3572 and TG3571 on the substrate are almost the same as that of InN samples TG3558 and TG3550 respectively, for which the growth rates are shown in Fig. 3-2. The detailed investigation of the composition of the film deposited on the growth substrate was not performed. However, the films deposited at lower AsH_3/N_2 ratio should contain nitrogen because the XRD profile for the TG3571 sample shows the diffraction from InN(200), although it is very small. All the diffraction peaks from the deposited films are very small, probably due to its amorphous-like property.

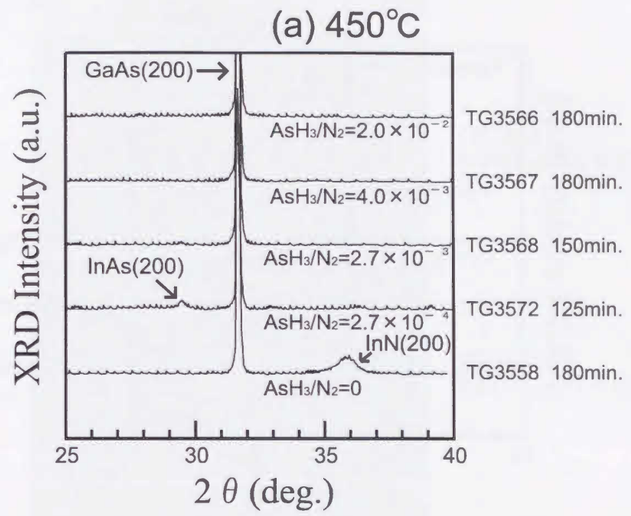

Figure 3-6(a). XRD profiles of the samples grown at 450℃.

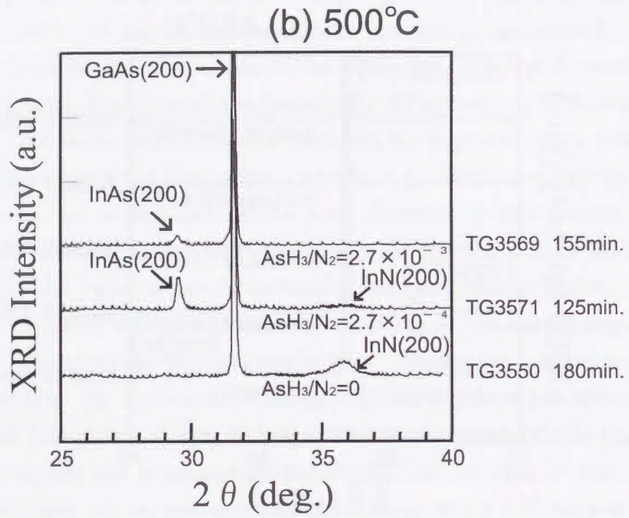

Figure 3-6(b). XRD profiles of the samples grown at 500℃.

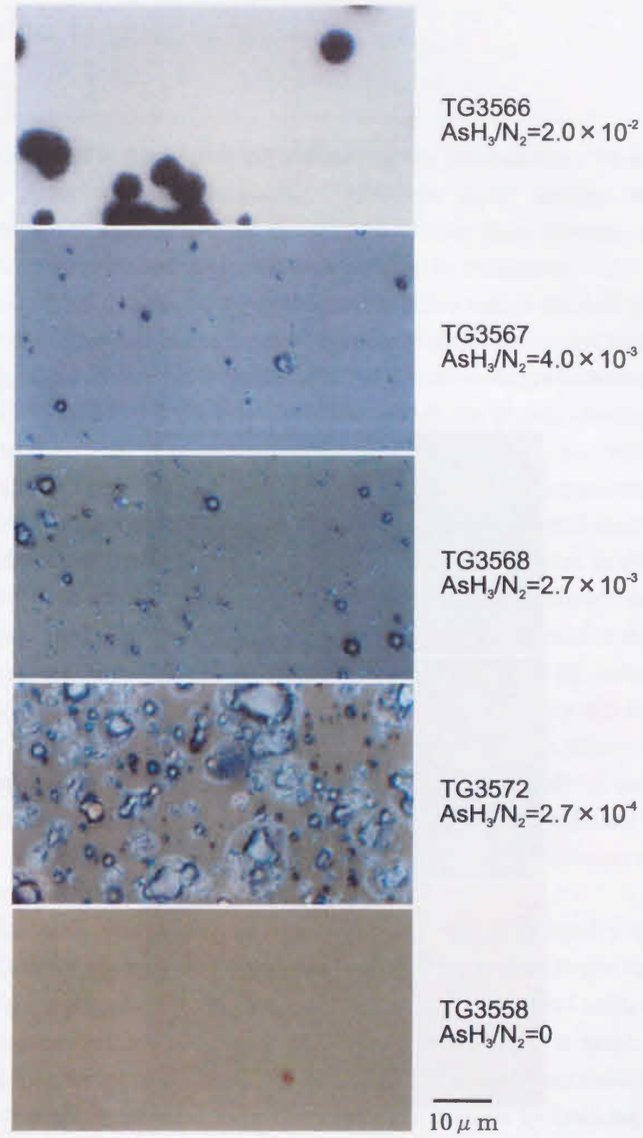

Figure 3-7(a). Surface micrographs of the samples grown at 450℃.

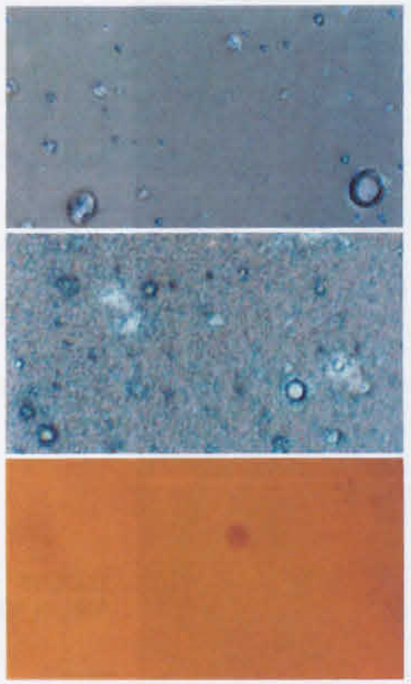

Figure 3-7(b). Surface micrographs of the samples grown at 500℃.

3-5 Discussion

The InN obtained in this growth experiment had very poor quality. Moreover, epitaxial InNAs phase was not obtainable. However, some features of this plasma-assisted MOCVD apparatus could be obtained. From these features, useful information for the modification of the growth apparatus can be withdrawn.

In the case of InN growth, no deposition on the inside wall in the bulk plasma region was observed. This was due to the etching effect of plasma-generated hydrogen radicals. Hydrogen radicals are easily produced in the growth environment because H_2 is less stable than N_2 [16, 17]. If the pressure is low enough, the plasma electrons can receive enough energy from the microwave electric field to dissociate most gas molecules via collision. However, the pressure used in this growth experiment is 3 Torr, and the mean free path of the electron is expected to be small (<< 1 mm) [18], resulting in a low mean electron energy. Of course, some of the electrons in the high energy tail of the Maxwell-Boltzmann energy distribution receive enough energy to decompose the N_2 molecules, and hence the nitrogen radicals exist in the bulk plasma. However, the highly energetic electrons also collide with H_2 molecules, producing hydrogen radicals as well as nitrogen radicals. Consequently the ratio of nitrogen radicals to the total amount of radicals decreases with the addition of H_2 molecules. After around ten InN growth experiments, the inside wall of the bulk plasma region became slightly frosted. This phenomenon can be also explained by the etching of quartz wall by hydrogen radicals, and hence, the oxygen was incorporated in InN films as revealed by XPS analysis [8].

When the AsH_3 was added into the plasma stream, As-related materials deposited in the bulk plasma region. In this case, the production of hydrogen radicals was expected to be suppressed due to the lower stability of AsH_3 compared to H_2 or N_2. That is, AsH_3 decomposes completely around 500-600℃ [19] and is much more breakable than NH_3 as shown in chapter 2, and NH_3 decomposes even more easily than H_2 or N_2 [17]. It could be possible to produce hydrogen radicals by cracking AsH_3 molecule. However, other species such as exited hydrogen molecule or ground state hydrogen molecule can also be produced by the decomposition of AsH_3 molecules. Two or three hydrogen radicals are not always produced from one AsH_3 molecule. The plasma, especially if it is made from many gas types, is a highly complex and reactive environment. The reactions in single gas plasmas, such as SiH_4 or CF_4, have been intensively investigated in the field of plasma engineering or science. Systematic

studies of the complex plasmas used herein have never been undertaken. Simplistically, it was expected that, in the macroscopic view, the amount of the hydrogen radicals in the bulk plasma should decrease by adding AsH_3, resulting in the suppression of quartz etching. And if the sticking coefficient of As-related species on the quartz is relatively high as compared to other possible species, the deposition on the wall even in the bulk plasma region is all the more enhanced when AsH_3 is present.

It is well known that small dust particles are formed in a wide variety of semiconductor processing plasma reactors that are typically operated around 1 Torr [20-23]. The elements forming the particles depend on the processing gases, and the diameter of the particles is in the range 0.01-1 μm. The initial nucleation of dust particles occurs by polymerization of the plasma species which can be neutral, positive, negative, or a combination of these (The path way is not well known yet, and it may well be that different plasma conditions favor different species.). Once these polymer nuclei have grown to nanometers in diameter, they are able to support more than one elementary charge. Then, the grains behave as electrically floating points in the bulk plasma. In our growth apparatus, the gas drift velocity is estimated to be around 2 m/s while the velocity of molecules based on thermal motion is around a few hundred meters per second. The mean free path of the gas molecule is a few tens of micrometers. Hence, each molecule or activated specie collides many times to form polymers or small particles before they come out of the bulk plasma, or until they reach the growth substrate. Since the gases were flowing though the cylindrical plasma in this growth apparatus, the residence time of each activated specie was relatively short as compared to that in the typical plasma process chamber. So, the particle was expected to reach the growth substrate before they grow big. InN, InAs, InNAs, carbon-related species and so on probably form the polymers or small particles. The nitrogen radical reaching the growth substrate is expected to be very low. The film on the growth substrate in this experiment is probably composed of those small polymer particles, resulting in the amorphous-like features of the film.

As the AsH_3/N_2 source ratio decreased, the deposition on the inside wall just downstream of the bulk plasma was suppressed and the deposition in the bulk plasma region became thinner. Simultaneously, the film growth rate on the substrate increased. This was probably due to the higher sticking coefficient of As-related species on the quartz as compared to other possible species. Thus, when the AsH_3 flow decreased, the deposition on the chamber wall decreased and more depositing species reached the substrate.

From the results and discussion above, some ideas for the modification of this plasma-assisted MOCVD apparatus can be obtained.

1) It is necessary to crack N_2 separately and to introduce into the growth chamber without previous mixing with other gases. This is to avoid the possible gas phase chemical reactions between activated species to form polymers, and to avoid the generation of hydrogen radicals that etch the chamber wall resulting in contamination of the film. Using the ideal gas model, the generated nitrogen radicals are expected to have a Maxwell-Boltzmann energy distribution, so some of them should have very high energy. Even if the nitrogen plasma is separately generated, the sputtering of the plasma enclosure could happen resulting in the contamination in the depositing film. The RF-nitrogen radical source mounted on MBE systems generally employs pyrolytic boron nitride (PBN) as a nitrogen plasma enclosure material to minimize contamination of the depositing films [24, 25]. Sato, in his plasma-assisted MOCVD experiments for the growth of InN [5] and GaNAs [4], used a quartz tube to enclose the microwave-exited nitrogen plasma. The contamination problem has not been reported in Sato's growth apparatus so far.

2) It is necessary to decrease the growth pressure. This is to suppress the recombination of nitrogen radicals in bulk plasma and downstream, and any other possible reactions between nitrogen radicals and other molecules in the growth chamber. Usually, the plasma-assisted MOCVD is performed at pressures of 0.1-1 Torr [1-5, 17, 26], depending on the dimension of the reactor, where the lifetime of the radicals is expected to be of the same order as the flight time of the radicals from the plasma cell to the growth substrate. The lifetime of the radicals generally depends on both total pressure and the radical density. Since extensive experimental investigation of the nitrogen plasma has not been performed, there is not enough information on parameters of the nitrogen radical production. Hence, the precise design of the plasma-assisted MOCVD reactor is impossible. However, it is clear that reducing the pressure (from 3 Torr) leads to the better results.

3-6 Conclusions

Growth of InNAs and InN was attempted by a plasma-assisted MOCVD experiment in which all the mixed source gases were cracked upstream of the substrate by microwave plasma excitation. Films containing the elements of In, N and As were deposited on the growth substrates. However, all these films had a poor quality with amorphous-like properties. No crystallized InNAs was obtained by this growth method. Grown InN films were almost amorphous with the zincblende phase in a slight majority. These poor results were attributed to the gas phase chemical reactions between activated source species to form polymers. Finally, it was concluded that the nitrogen radicals hardly reached the growth substrate and did not contribute to the film deposition, though InN growth was first performed in an attempt to make sure that the nitrogen radical was reaching the growth substrate. The necessity of the separate production of nitrogen radicals and its separate introduction into the growth chamber at reduced pressure was pointed out for the growth of good quality InNAs or InN.

References

[1] A. Wakahara, T. Tsuchiya and A. Yoshida: Vacuum **41**, (1990) 1071.

[2] A. Wakahara and A. Yoshida: Appl. Phys. Lett. **54**, (1989) 709.

[3] Q. Guo, H. Ogawa, H. Yamamoto and A. Yoshida: Appl. Phys. Lett. **66**, (1995) 715.

[4] M. Sato: J. Cryst. Growth **145**, (1994) 99.

[5] M. Sato: Jpn. J. Appl. Phys. **36**, (1997) L595.

[6] H. Naoi, Y. Naoi and S. Sakai: 1996 Shikoku-Section Joint Convention Record of The Institutes of Electrical and Related Engineers, p. 139 (11-17) [in Japanese].

[7] Presented in the convention of Ref. [6].

[8] T. Yang, Y. Naoi, H. Naoi and S. Sakai: Proc. Int. Symp. on Blue Laser and Light Emitting Diodes, 1996, eds. A. Yoshikawa et al. (Ohmsha, Tokyo, 1996) p.504.

[9] S. Porowski and I. Grzegory: J. Crystal Growth **178** (1997) 174.

[10] J. B. MacChesney, P. M. Bridenbaugh and P. B. O'Connor: Mater. Res. Bull. **5** (1970) 783.

[11] F. A. Ponce: Mater. Res. Bull. **22** (1997) 51.

[12] S. Strite, D. Chandrasekhar, David J. Smith, J. Sariel, H. Chen, N. Teraguchi and H. Morkoc: J. Cryst. Growth **127**, (1993) 204.

[13] D. Chandrasekhar, D. J. Smith, S. Strite, M. E. Lin and H. Morkoc: J. Cryst. Growth **152**, (1995) 135.

[14] A. Yamamoto, Y. Yamauchi, M. Ohkubo and A. Hashimoto: J. Cryst. Growth **174**, (1997) 641.

[15] See, for example, C. Kittel: *Introduction to Solid State Physics*, 7th edition (John Wiley & Sons, New York, 1996) pp. 17-18 (Chapter 1).

[16] See, for example, *CRC Handbook of Chemistry and Physics*, 69th edition (CRC Press, Boca Raton, Florida, 1988), F-176, F-177.

[17] M. Sato: Solid State Electron. **41**, (1997) 223.

[18] B. Chapman: *Glow Discharge Processes*, 1st edition (John Wiley & Sons, New York, 1980), and M. A. Lieberman and A. J. Lichtenberg: *Principles of Plasma Discharges and Materials Processing*, 1st edition (John Wiley & Sons, New York, 1994).

[19] G. B. Stringfellow: *Organometallic Vapor-Phase Epitaxy: Theory and Practice*, 1st edition (Academic Press, San Diego, 1989) pp.170-171 (Chapter 4).

[20] Bull. of The American Physical Society Vol. **45**; Program of The 53rd Annual Gaseous Electronics Conference (GEC2000 Meeting), pp.65-66.

[21] P. Haaland, S. Ibrani and H. Jiang: Appl. Phys. Lett. **64**, (1994) 1629.

[22] P. Haaland, A. Garscadden and B. Ganguly: Appl. Phys. Lett. **69**, (1996) 904.

[23] U. Kortshagen: Appl. Phys. Lett. **71**, (1997) 208.

[24] W. E. Hoke, P. J. Lemonias and D. G. Weir: J. Cryst. Growth **111**, (1991) 1024.

[25] C. T. Foxon, T. S. Cheng, S. V. Novikov, D. E. Lacklison, L. C. Jenkins, D. Johnston, J. W. Orton, S. E. Hooper, N. Baba-Ali, T. L. Tansley and V. V. Tret'yakov: J. Cryst. Growth **150**, (1995) 892.

[26] M. Weyers and M. Sato: Appl. Phys. Lett. **62**, (1993) 1396.

Chapter 4
Growth of InNAs by MBE

4-1 Introduction

Among the several crystal growth methods, molecular beam epitaxy (MBE) provides growth conditions farthest from equilibrium. MBE involves the reaction of thermally effused beams of atoms or fragile molecules with a crystalline surface under ultrahigh vacuum (UHV) conditions at relatively low substrate temperatures. Consequently, the driving force for material formation or growth in MBE is relatively strong as compared to that in other growth methods. Hence, MBE is favorable for the growth of materials that have a large compositional miscibility gap such as III-N-V alloys. Because of the UHV conditions, MBE is well suited to in situ growth monitoring by techniques such as reflective high energy electron diffraction (RHEED) and mass spectroscopy (MS). In situ growth monitoring is necessary especially for the growth of materials requiring precise control of the growth conditions. MBE growth of nitrogen-containing III-V compounds usually employs plasma-cracked nitrogen as the N source. Due to the use of nitrogen gas, the pressure in the MBE chamber during N-containing material growth becomes higher than that for III-V compounds not containing nitrogen, even though the N_2 flow rate is very low (typically less than 10 sccm [1] at the maximum). However, by carefully maintaining the chamber pressure below ~ 10^{-4} Torr when using a plasma nitrogen source [1], the mean free path of the source species is greater than ~ 80 cm, whereas the distance between the source cells and the growth substrate is around 20 cm [2]. Hence, the gas phase chemical reactions between plasma-cracked reactive nitrogen and other source species can be avoided, which is very important for high quality crystal growth as mentioned in chapter 3.

Additionally, at chamber pressure below ~ 10^{-4} Torr, the in situ growth monitoring techniques discussed above are still available. So, MBE is widely used for the growth of not only III-N-V alloys [3-13] but also zincblende GaN [14-18], InN [14,19,20], $Al_xGa_{1-x}N$ [21] and $Ga_xIn_{1-x}N$ [22-24] that preferably have the wurtzite structure. Hence, poly-crystal or even near single crystalline wurtzite structures are achieved by small deviations in the growth conditions.

In this chapter, MBE growth of InNAs using a radio frequency (RF) nitrogen radical source is presented. This work was accomplished under collaboration with the University of Nottingham. Successful growth of $InN_{0.38}As_{0.62}$ almost lattice-matched to a (100)GaAs substrate is demonstrated [25]. The growth conditions are optimized using RHEED.

4-2 Growth apparatus and sample preparation

All MBE growth herein was performed in a conventional Varian modular GenII MBE system equipped with an Oxford Research CARS 25 RF activated plasma N source and solid sources of Ga, Al, In, As_2, Si and Be. A schematic representation of the MBE growth apparatus is shown in Fig. 4-1. The detailed description of the RF activated plasma N source is given elsewhere [15].

Semi-insulating (100)GaAs ready for epitaxial growth was used as a substrate. After introduced into the growth chamber, the substrates were annealed in a flux of arsenic at 620℃ to remove the surface oxide. MBE growth was performed at 500℃ using a solid In, an As cracker to produce As_2 and plasma-cracked nitrogen. The flux of active nitrogen was monitored by the optical emission detector (OED) consisting of a silicon photodiode sensor with a spectral peak response at approximately 850 nm and an integrated circuit current-to-voltage converter that gives an output voltage proportional to illumination. The relation between the amount of active nitrogen (OED output voltage) so measured and the flow rate of nitrogen into the plasma cell at various RF excitation powers is given in Ref. [15]. The OED signal is proportional to the amount of active nitrogen species coming from the plasma source [26]. After a GaAs buffer layer was grown on the substrate at 500℃, the Ga shutter was closed and the In and N shutters were opened at the same time. Upon completion of the deposition process, the

In shutter was closed, while N and As shutters were kept opened until the substrate temperature fell below 300℃. The growth conditions are summarized in table 4-1.

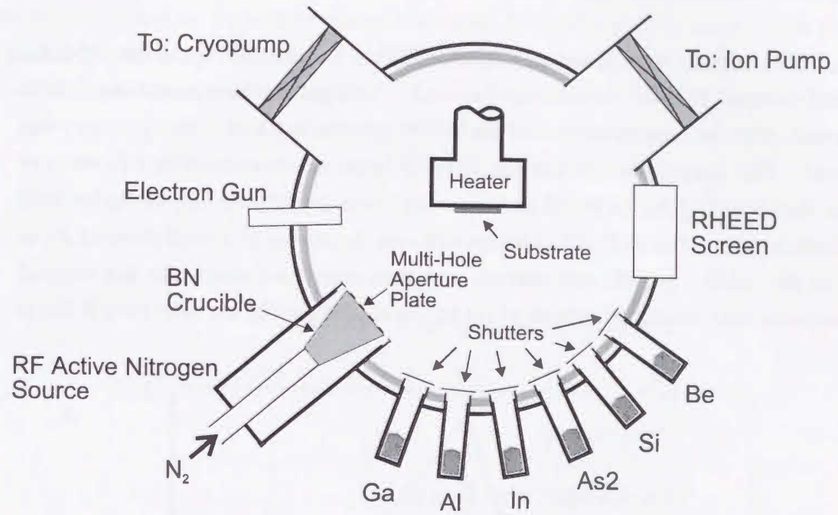

Figure 4-1. Schematic representation of the MBE growth apparatus.

Table 4-1. Growth conditions.

Substrate	(100)GaAs ready for epitaxial growth
In	$2\sim4\times10^{-7}$ Torr
As	$1\sim12\times10^{-6}$ Torr
N	$\sim1\times10^{-5}$ Torr, OED = 0~0.8V
Growth Temperature	500℃
Pressure	$\sim1\times10^{-5}$ Torr

4-3 Results and discussion

4-3-1 Growth monitoring

The growth was monitored by RHEED. During the GaAs growth, the expected streaked RHEED pattern was observed. This pattern disappeared about 10 to 20 seconds after the commencement of the InNAs growth, and a new, spotty pattern was observed. The intensity of the specular RHEED beam was monitored as a function of time as shown in Fig. 4-2, in which an InNAs layer was grown for 5 seconds in between two GaAs layers. The RHEED intensity suddenly decreased to a level denoted R_1 as soon as the InNAs growth was started, and then recovered almost to the original intensity observed during the growth of GaAs, denoted R_0. The intensity ratio R_1/R_0 is

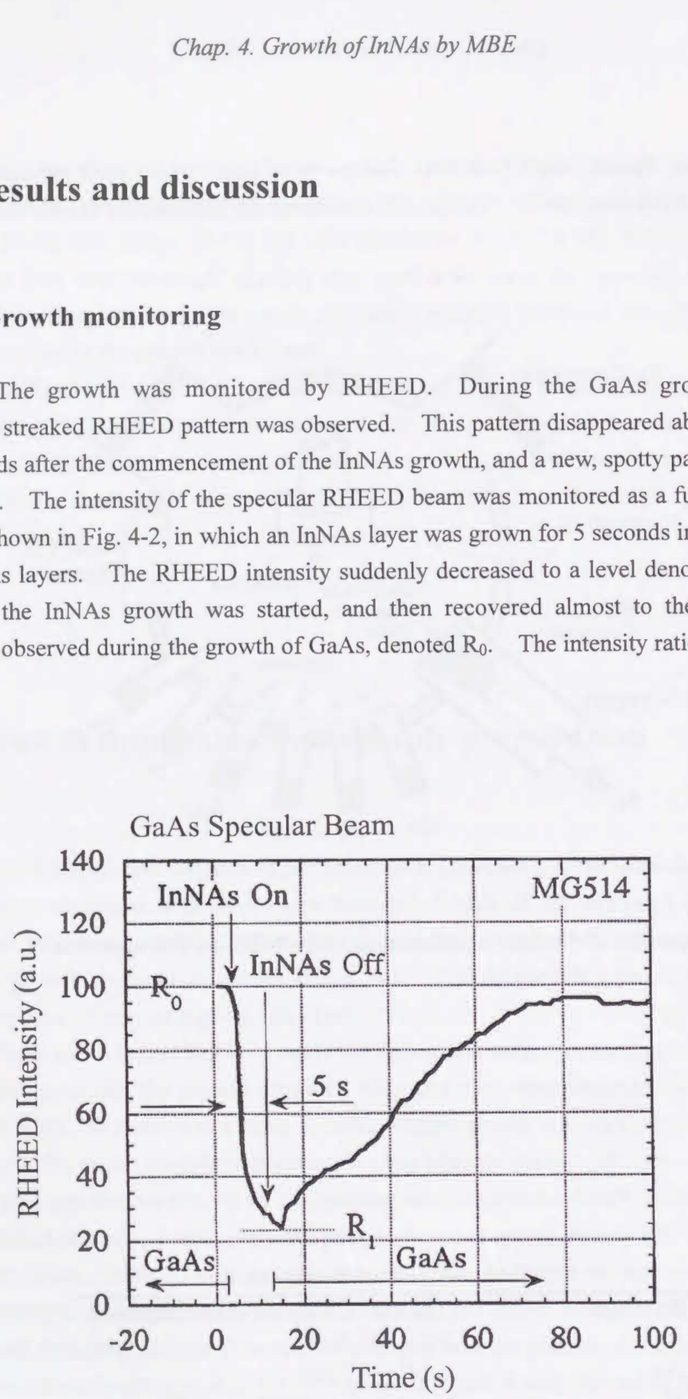

Figure 4-2. RHEED intensity as a function of time.

plotted as a function of the N/As flux ratio as shown in Fig. 4-3, where the relative N/As flux ratio was defined as the OED signal (volts) / As flux (Torr) $\times$ 10^{-4}. In the experimental results shown in Fig. 4-3, the As flux was kept constant at 4×10^{-6} Torr and OED was changed. The intensity ratio R_1/R_0 has a clear dependence on N/As flux ratio and has a maximum at OED = 0.6 V (N/As ratio = 15). The decay in RHEED intensity is caused by the lattice mismatch between the InNAs and the GaAs. The time constant for the decay increased as the lattice matching condition was approached and was the longest for a N/As ratio of 15.

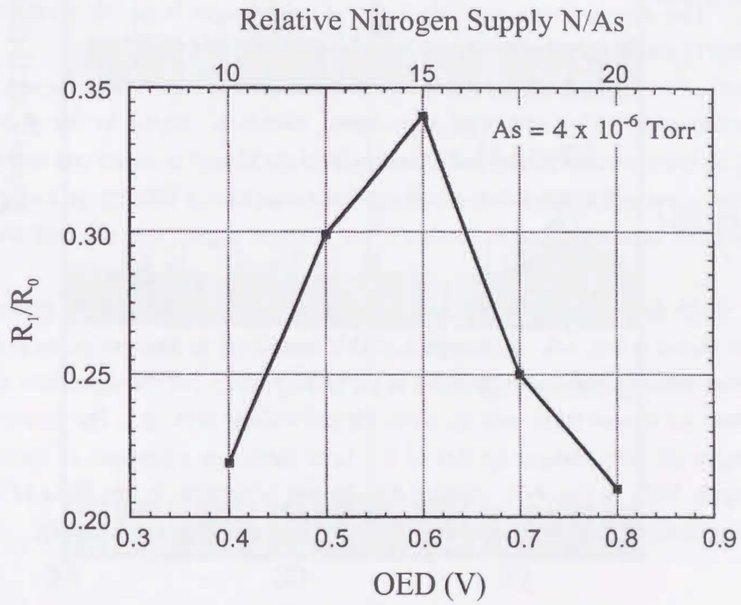

Figure 4-3. R_1/R_0 versus OED. The lines are used only to guide the eye.

4-3-2 Properties of grown InNAs

The grown layers were characterized by scanning electron microscopy (SEM), energy dispersive x-ray spectroscopy (EDX), x-ray diffraction (XRD) and secondary ion mass spectrometry (SIMS).

InNAs layers were grown on GaAs at different N/As flux ratios. A XRD system (Philips, X'Pert, Type: PW3040/00) using the radiation of Cu $K\alpha_1$ coming through Ge(220) quadru-crystal monochromator was used herein. The XRD patterns of the resultant layers near GaAs (200) and (400) diffraction peaks are shown in Fig. 4-4(a) and (b), respectively. When the N/As ratio is too low, only a broad peak of an InAs and a sharp GaAs peak are visible, while a broad InN(200) peak also appears at N/As=80. In addition to these peaks, a peak close to the GaAs(400) is clearly visible when N/As ratio is 15. This ratio is the same as that which gives the longest RHEED decay time. The average grown layer thickness of each sample is 80, 30, 80 nm for MG510, MG515 and MG509, respectively.

Surface micrographs taken by SEM are shown in Fig. 4-5. The surface of MG515, however, is milky with triangular-shaped islands as shown in the figure. EDX mapping indicates that In, As, and N exist within the triangular island and that the outside of the island is GaAs. White pits shown on the surface of MG509 are found to be InN by EDX analysis. On the contrary, no nitrogen signal was detected from MG510.

A SIMS depth profile measurement was performed using O_2^+ as the primary ion beam as shown in Fig. 4-6. Although the SIMS sensitivity to nitrogen atoms is not strong, a clear nitrogen signal was detected in the ternary layer. A Ga signal was also detected, since the ternary layer does not cover the entire GaAs surface. The measured SIMS nitrogen intensity divided by that of the In is shown as a function of relative nitrogen supply N/As in Fig. 4-7. Almost no nitrogen is detected below N/As of 10, and the nitrogen signal intensity increases with increasing relative nitrogen supply.

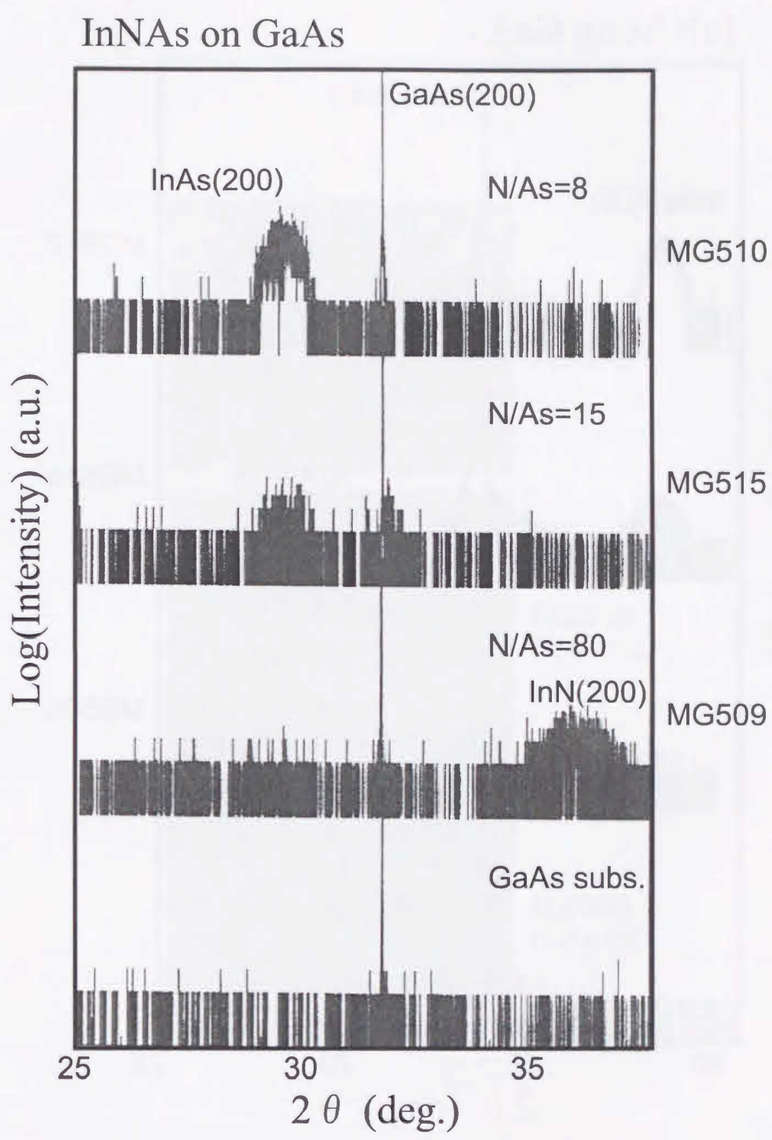

Figure 4-4(a). XRD near GaAs(200) diffraction peak.

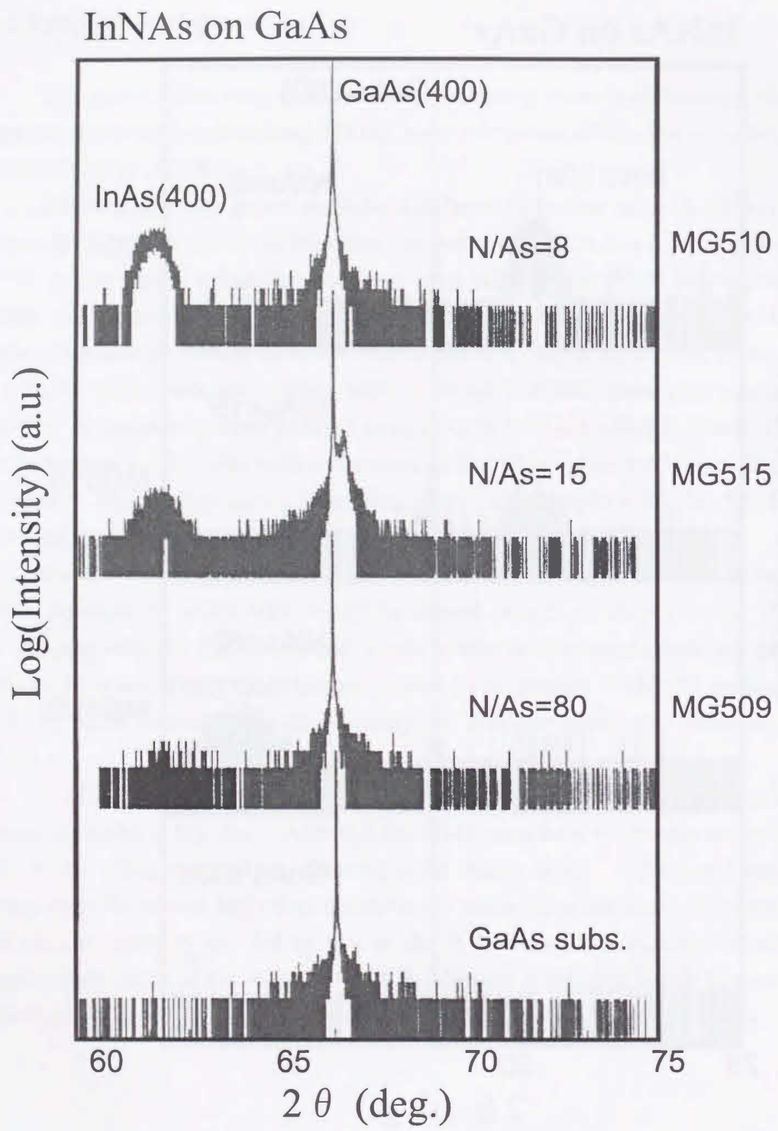

Figure 4-4(b). XRD near GaAs(400) diffraction peak.

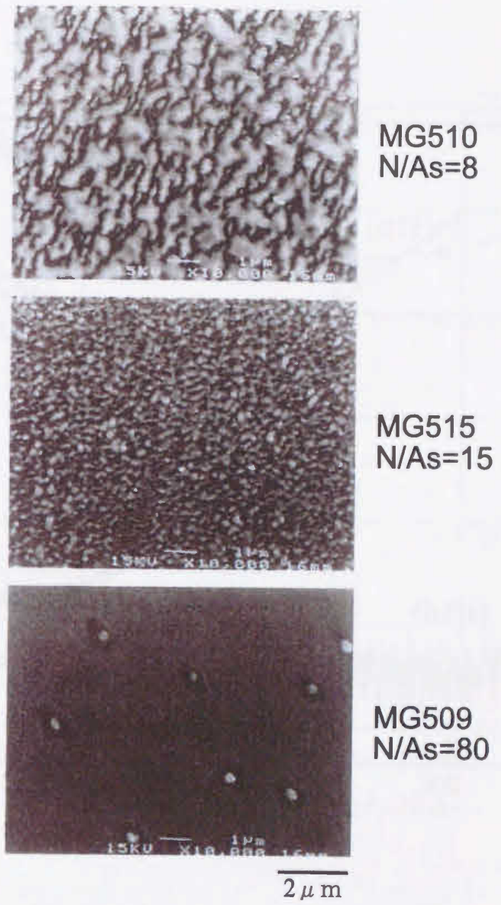

Figure 4-5. Surface microphotographs of the grown layers.

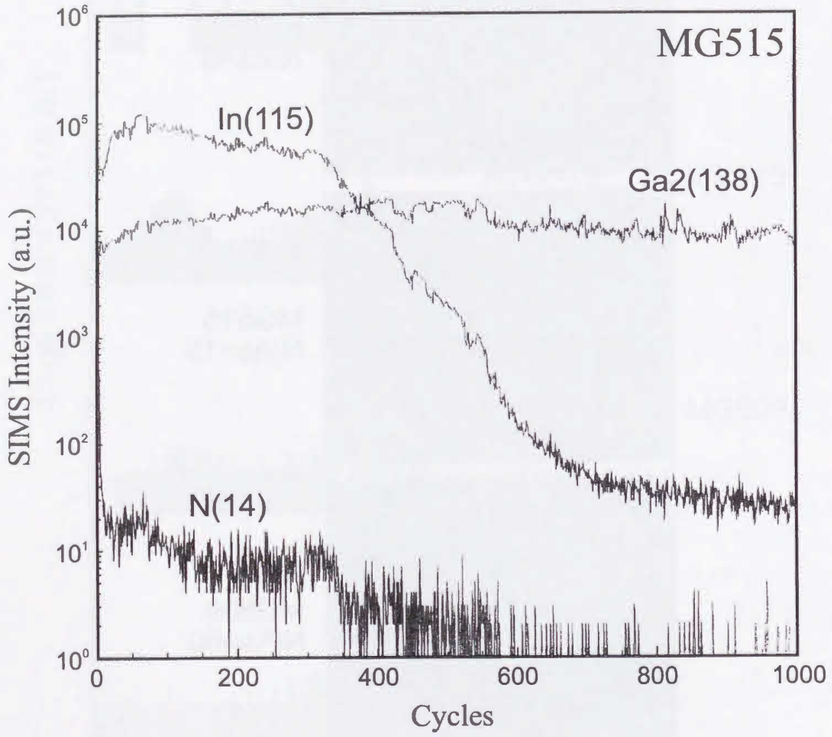

Figure 4-6. In-depth SIMS profile of the sample MG515.

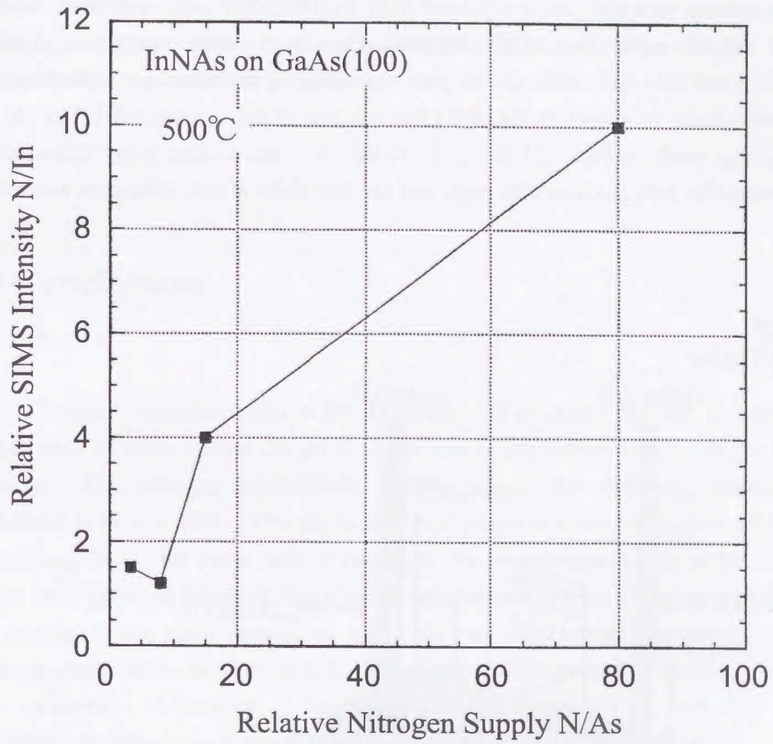

Figure 4-7. Relative nitrogen intensity as a function of nitrogen supply. The lines are used only to guide the eye.

Summarizing these results, it can be concluded that InNAs can be grown only when its lattice constant is close to that of the GaAs substrate. Assuming the Vegard's law, the nitrogen content of InNAs in MG515 is estimated to be 0.38. As a matter of course, the properties of InNAs become close to that of InN as the nitrogen composition increases. It was speculated that the $InN_{0.38}As_{0.62}$ layer might contain the wurtzite phase with the [0001] direction parallel to the zincblende <111> crystal direction as mentioned for InN in sub-section 3-3-4. In order to investigate the crystal structure of this $InN_{0.38}As_{0.62}$ material, an x-ray ω-2θ (θ-2θ) scan was measured while changing the tilt angle (Psi) of the sample. Only peaks from zincblende GaAs, $InN_{0.38}As_{0.62}$ and InAs were seen, and no peak was visible at the points corresponding to the wurtzite phase, as shown in Fig. 4-8 (The position of the wurtzite $(10\bar{1}0)$ or $(01\bar{1}0)$$InN_{0.38}As_{0.62}$ peak is: Psi~$\pm$35.26° , θ~12.90° .). An ω-scan x-ray diffraction was measured for $InN_{0.38}As_{0.62}$(400) peak, and the full width at half maximum was 350 arcsec.

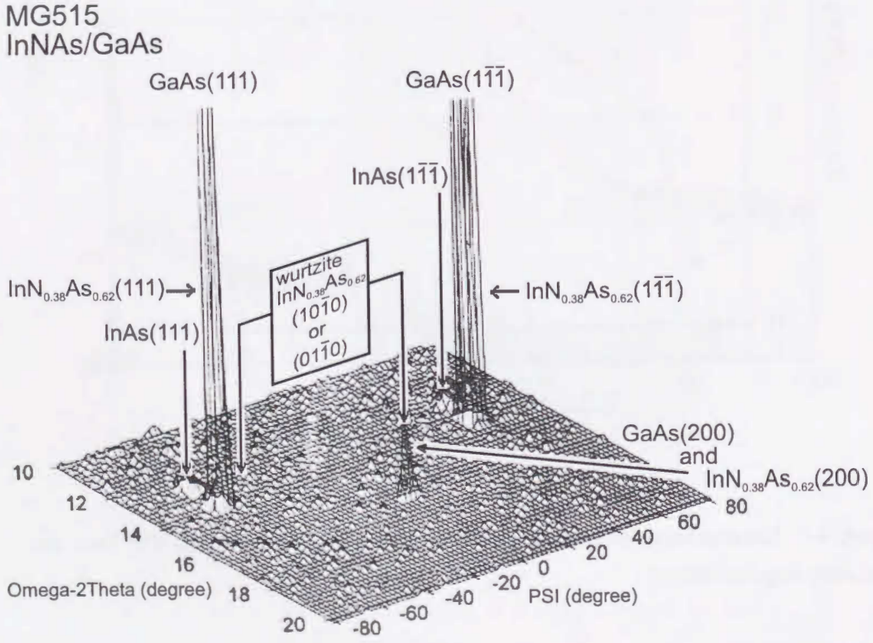

Figure 4-8. 3D XRD profile of the sample MG515.

The $InN_{0.38}As_{0.62}$ is theoretically predicted to have a negative band gap energy (semi-metallic property) [27, 28]. Due to the discontinuity of $InN_{0.38}As_{0.62}$ layer synthesized in this growth experiment, the resistivity of the layer could not be measured. Kao et al. also synthesized $InN_{0.38}As_{0.62}$ by MBE using an electron cyclotron resonance (ECR) nitrogen plasma source [27]. They applied Hall effect measurement to the grown films and obtained typical Hall mobility of 50-100 cm^2/Vs with a high carrier density of ~1×10^{20} cm^{-3}, though the surface was rough. No photoluminescence was observed from the films. These facts indicate $InN_{0.38}As_{0.62}$ may be semi-metallic. The $InN_{0.38}As_{0.62}$ layer grown in this experiment, though not a continuous film, is also expected to have semi-metallic properties.

4-4 Conclusions

It was demonstrated that an InNAs layer could be grown by MBE by adjusting the flux ratio of N/As so that the grown layer was nearly lattice-matched to the GaAs substrate. The nitrogen solid phase composition of the InN_xAs_{1-x} grown was determined to be x = 0.38. Though no electrical properties were obtainable from this $InN_{0.38}As_{0.62}$ layer, the layer was expected to have semi-metallic properties. The ternary layer grown in this study had a rough surface and included phase-separated InAs. The details of this phase separation and a way to suppress the occurrence of this phase-separated InAs are given in Ref. [29], which was performed by another group in the author's laboratory employing a super-lattice structure of GaAs(40nm)/$InN_{0.38}As_{0.62}$(0.4nm) with seven periods.

References

[1] W. E. Hoke, P. J. Lemonias and D. G. Weir: J. Cryst. Growth **111**, (1991) 1024.

[2] For example, 15~17 cm in Varian MBE system, 24 cm in Eiko-EV100S MBE system.

[3] J. N. Baillargeon, K. Y. Cheng, G. E. Hofler, P. J. Pearah and K. C. Hsieh: Appl. Phys. Lett. **60**, (1992) 2540.

[4] W. G. Bi and C. W. Tu: Appl. Phys. Lett. **69**, (1996) 3710.

[5] K. Iwata, H. Asahi, K. Asami and S. Gonda: J. Cryst. Growth **175/176**, (1997) 150.

[6] H. P. Xin, C. W. Tu, Y. Zhang and A. Mascarenhas: Appl. Phys. Lett. **76**, (2000) 1267.

[7] W. Shan, W. Walukiewicz, K. M. Yu, J. Wu, J. W. Ager III, E. E. Haller, H. P. Xin and C. W. Tu: Appl. Phys. Lett. **76**, (2000) 3251.

[8] W. G. Bi and C. W. Tu: J. Appl. Phys. **80**, (1996) 1934.

[9] W. G. Bi and C. W. Tu: Appl. Phys. Lett. **70**, (1997) 1608.

[10] K. Uesugi and I. Suemune: J. Cryst. Growth **189/190**, (1998) 490.

[11] S. Francoeur, G. Sivaraman, Y. Qiu, S. Nikishin and H. Temkin: Appl. Phys. Lett. **72**, (1998) 1857.

[12] K. Uesugi, I. Suemune, T. Hasegawa, T. Akutagawa and T. Nakamura: Appl. Phys. Lett. **76**, (2000) 1285.

[13] M. Kondow, K. Uomi, A. Niwa, T. Kitatani, S. Watahiki and Y. Yazawa: Jpn. J. Appl. Phys. **35**, (1996) 1273.

[14] D. Chandrasekhar, D. J. Smith, S. Strite, M. E. Lin and H. Morkoc: J. Cryst. Growth **152**, (1995) 135.

[15] C. T. Foxon, T. S. Cheng, S. V. Novikov, D. E. Lacklison, L. C. Jenkins, D. Johnston, J. W. Orton, S. E. Hooper, N. Baba-Ali, T. L. Tansley and V. V. Tret'yakov: J. Cryst. Growth **150**, (1995) 892.

[16] O. Brandt, H. Yang, A. Trampert, M. Wassermeier and K. H. Ploog: Appl. Phys. Lett. **71**, (1997) 473.

[17] S. Ruvimov, Z. L. -Weber, J. Washburn, T. J. Drummond, M. Hafich and S. R. Lee: Appl. Phys. Lett. **71**, (1997) 2931.

[18] H. Okumura, H. Hamaguchi, G. Feuillet, Y. Ishida and S. Yoshida: Appl. Phys. Lett. **72**, (1998) 3056.

[19] S. Strite, D. Chandrasekhar, David J. Smith, J. Sariel, H. Chen, N. Teraguchi and H. Morkoc: J. Cryst. Growth **127**, (1993) 204.

[20] A. Tabata, A. P. Lima, L. K. Teles, L. M. R. Scolfaro, J. R. Leite, V. Lemos, B. Schottker, T. Frey, D. Schikora and K. Lischka: Appl. Phys. Lett. **74**, (1999) 362.

[21] H. Harima, T. Inoue, S. Nakashima, H. Okumura, Y. Ishida, S. Yoshida, T. Koizumi, H. Grille and F. Bechstedt: Appl. Phys. Lett. **74**, (1999) 191.

[22] J. R. Mullhauser, B. Jenichen, M. Wassermeier, O. Brandt and K. H. Ploog: Appl. Phys. Lett. **71**, (1997) 909.

[23] J. R. Mullhauser, O. Brandt, A. Trampert, B. Jenichen and K. H. Ploog: Appl. Phys. Lett. **73**, (1998) 1230.

[24] E. Silveira, A. Tabata, J. R. Leite, R. Trentin, V. Lemos, T. Frey, D. J. As, D. Schikora and K. Lischka: Appl. Phys. Lett. **75**, (1999) 3602.

[25] S. Sakai, T. S. Cheng, T. C. Foxon, T. Sugahara, Y. Naoi and H. Naoi: J. Cryst. Growth **189/190**, (1998) 471.

[26] S. V. Novikov, A. J. Winser, I. Harrison, C. S. Davis and C. T. Foxon: Semicond. Sci. Technol. **15** (2000) 1.

[27] Y. C. Kao, T. P. E. Broekaert, H. Y. Liu, S. Tang, I. H. Ho and G. B. Stringfellow: Mater. Res. Soc. Symp. Proc. Vol. **423**, (1996) pp. 335-340, and the references therein.

[28] T. Yang, S. Nakajima and S. Sakai: Jpn. J. Appl. Phys. **36**, (1997) L320.

[29] M. Hao, S. Sakai, T. Sugahara, T. S. Cheng and C. T. Foxon: J. Cryst. Growth **189/190**, (1998) 481.

Chapter 5
Growth of InNAs by low-pressure MOCVD employing plasma-cracked nitrogen and in situ generated arsine radicals

5-1 Introduction

Following the ideas suggested in chapter 3, TMIn, arsine and pre-cracked nitrogen are separately introduced into a MOCVD growth chamber, without previous mixing, for the growth of InNAs. A low production rate plasma arsine generator provides arsine radicals to the growth system, increasing N/As source flux ratio with the goal of synthesizing InNAs with a high nitrogen solid phase composition. The InNAs grown by this approach is characterized [1]. InAs is also grown by employing the in situ generated arsine radicals. The results of the InAs growth are also presented [2]. This work was accomplished under collaboration with Colorado State University.

5-2 Growth apparatus

The in situ generation of arsine is accomplished by reacting a microwave-exited hydrogen plasma with solid arsenic located slightly down stream of the active plasma region. A diagram of the growth apparatus is shown in Fig. 5-1. The solid arsenic is located about 3 cm downstream of an Evenson microwave cavity [3] which is connected to a 2.45 GHz microwave power supply (Opthos MPG-4M, 2.45 GHz) via coaxial cable. The plasma-generated arsine radicals (AsH, AsH_2, etc.) are delivered to the growth substrate through a 10 mm inside diameter quartz tube. Atomic nitrogen is produced from nitrogen gas using the same type of microwave cavity and delivered directly to the growth region via quartz tubing in a similar manner as the arsine radicals. The TMIn feedstock is introduced into the growth chamber using hydrogen carrier gas.

Semi-insulating (100)GaAs, misoriented by 2° towards [001], was used as a substrate for all the growth experiments presented in this chapter.

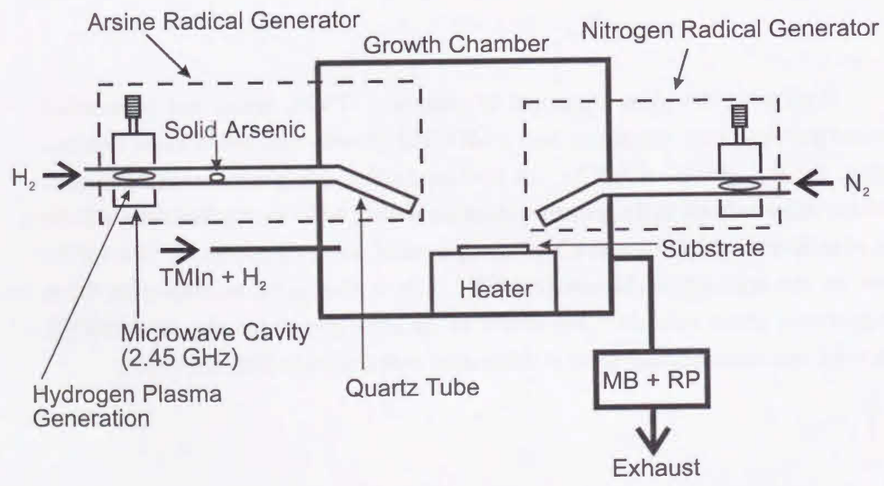

Figure 5-1. Schematic representation of the low-pressure MOCVD growth apparatus, including the in situ arsine and nitrogen radical generator.

5-3 Arsine delivery rate

The arsine delivery rate was investigated by connecting a mass spectrometer (Inficon Quadrex 200) to the growth chamber. The hydrogen flow rate through the arsine generator was varied from 25 to 100 sccm, and the microwave power was varied over the range of 15 - 70 W. Additional H_2 flow was provided to the chamber such that the total flow rate of hydrogen into the growth chamber was fixed at 100 sccm. The total pressure in the chamber was maintained at 750 mTorr during the experiment to achieve a constant residence time of the gas molecules in the chamber. The arsine delivery rate was determined from the sum of the arsine peak intensities monitored by the mass spectrometer, that is, the sum of the measured As, AsH, AsH_2 and AsH_3 peaks. Conversion from mass spectra peak intensities into sccm units was accomplished by measuring the difference in total mass of the solid arsenic piece and the generator apparatus both before and after **an hour of** operation at 40 W microwave power and 25 sccm hydrogen flow. The delivery rate of arsine into the chamber was determined to be 0.50 sccm for this operating condition. The details of the measurement procedure are given in Ref. [4]. The measured arsine delivery rates in sccm are shown in Fig. 5-2. No plasma is ignited or sustained below 10 W microwave power. The arsine delivery rate at each H_2 flow rate increases with increasing microwave power from 15 to 40 W, then begins to saturate, and increases again above 60 W. The saturated delivery rates of 0.53, 0.77, and 1.05 sccm, obtained at 55 W for H_2 flows of 25, 50 and 100 sccm respectively, are employed for all the film growth experiments discussed in this chapter.

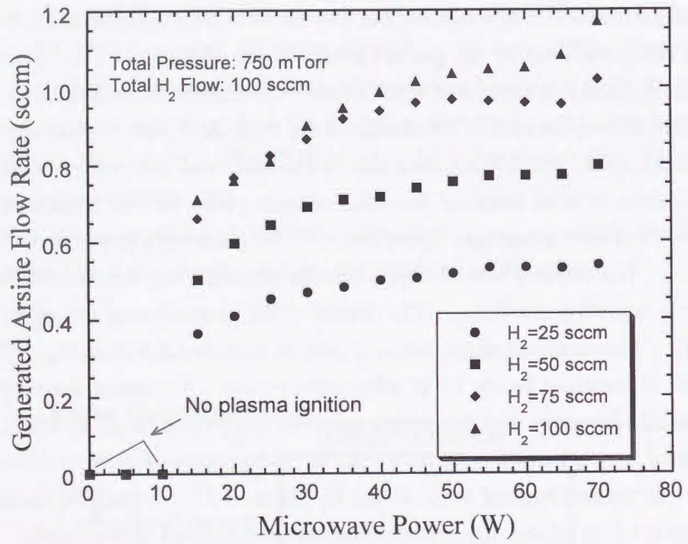

Figure 5-2. Arsine delivery rate vs. microwave power for each H_2 flow rate.

5-4 Growth of InAs

5-4-1 Motivation for InAs growth

The growth of group III arsenide material with in situ generation of arsine radicals is not widely reported. To the best of the author's knowledge, only Pihlstrom et al. of the co-researcher's group at Colorado State University (CSU) have demonstrated GaAs growth using in situ generated arsine [4, 5]. The CSU group used the same arsine radical generator as shown in Fig. 5-1. Initially, InAs growth was attempted herein using this unusual As source because InNAs can not be obtained without successful growth of InAs. Through the joint research program, single crystalline InAs films were obtained employing, for the first time, in situ plasma-generated arsine radicals [2]. In this section, the results of InAs growth are presented.

5-4-2 Sample preparation

The growth of InAs was performed using the same growth system (see Fig. 5-1.) without the nitrogen radical source.

The treatment of the substrate before the growth process was the same as discussed in section 2-2, with additional substrate annealing at 575℃ for 30 minutes in the in situ generated arsine ambient. After the substrate was adjusted to growth temperature, TMIn was introduced into the growth chamber. The InAs was grown directly on the GaAs substrate without any pre-growth of GaAs or other buffer layers. The growth conditions are summarized in table 5-1. The average V/III ratio in the growth chamber is estimated to be approximately 7 in these conditions. Upon completion of the film deposition process, the TMIn flow to the growth chamber was stopped, while the arsine production was continued until the substrate temperature fell below 300℃.

Table 5-1. Growth conditions for InAs.

Substrate	2° off GaAs(100)
Growth Temperature	350-550℃
TMIn	0.141 sccm
In situ Generated Arsine	1.05 sccm
H_2(total)	300 sccm
Pressure	750 mTorr
Growth Duration	60 minutes

5-4-3 Results and discussion

The grown layers were characterized by x-ray diffraction (XRD) and secondary ion mass spectrometry (SIMS).

The variation of the InAs growth rate with substrate temperature is shown in the Arrhenius plot of Fig. 5-3. The surface micrographs of the corresponding InAs samples are shown in Fig. 5-4. The error bar in Fig. 5-3 indicates the uncertainty in measuring the film thickness due to surface roughness at higher growth temperature as shown in Fig. 5-4. The sample grown at 450℃ had a specular, mirror-like surface when viewed with the naked eye. No indium droplet formation on the surface was observed in any of the samples.

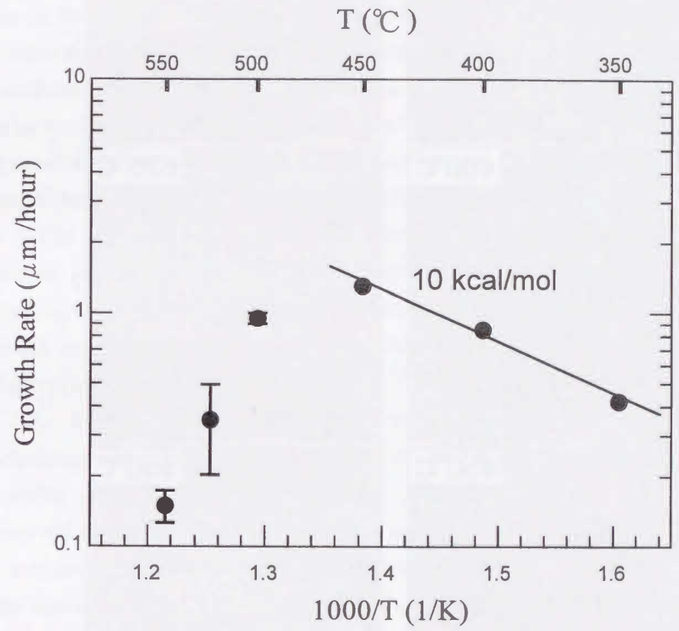

Figure 5-3. Growth rate of InAs vs. reciprocal temperature.

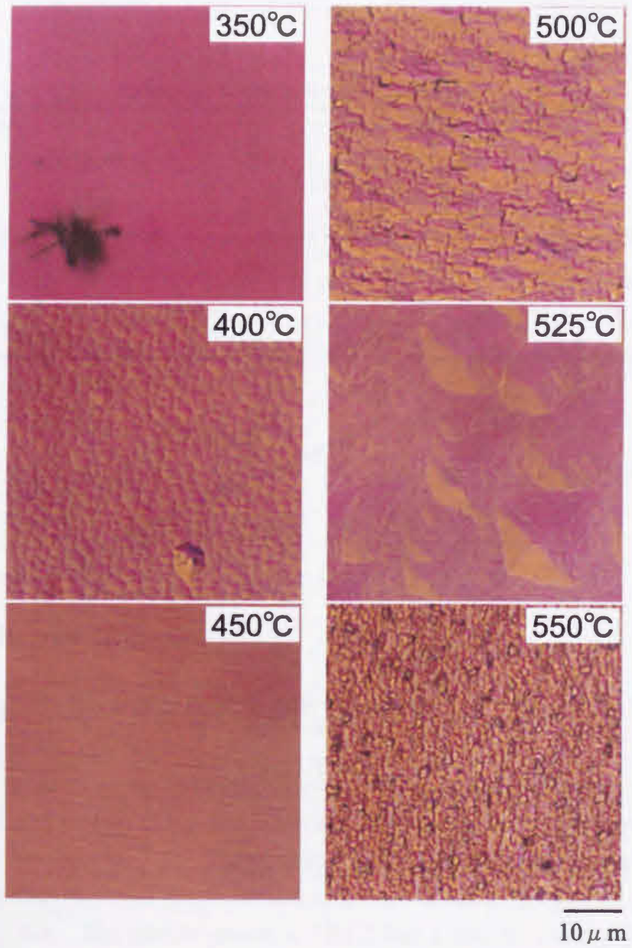

Figure 5-4. Surface micrographs of InAs samples.

The growth rate never becomes constant, but peaks at 450℃. The activation energy in the temperature range from 350℃ to 450℃ is approximately 10 kcal/mol. The growth rate decreases very rapidly above 500℃, probably due to the enhanced desorption of the feed species from the substrate at higher growth temperature in this low-pressure MOCVD chamber. In addition, possible etching of the depositing InAs by hydrogen radicals might be enhanced at higher temperature. Ma et al. reported a clear distinction between the kinetically controlled regime and the mass transport regime of InAs growth using TMIn and AsH_3 in atmospheric pressure MOCVD [6]. In their report, the growth rate increased at an activation energy of 24kcal/mol with increase in the growth temperature up to 400℃ and completely saturated above this temperature up to 600℃, explained by the complete TMIn decomposition. The value of 10 kcal/mol in Fig. 5-3 is much lower than their value of the kinetically controlled regime as well as the TMIn decomposition activation energy [7]. TMIn is completely decomposed above about 350℃ in a H_2 ambient as well [7], so the growth rate is expected to be mass transport limited from 350℃ to 450℃ in the MOCVD conditions herein. The observed increase in InAs growth rate with increase in the growth temperature is probably due to the enhanced diffusivity of the feed species in the boundary layer at higher temperature. From the discussion above, it is expected that the growth rate would be kinetically controlled by TMIn decomposition below 350℃ in this growth apparatus.

A θ -2 θ mode XRD measurement was performed with a powder diffractometer using the radiation of Cu Kα_1 and Kα_2. Figure 5-5 represents the XRD profile of the sample grown at 450℃. The two peaks from (200) and (400)InAs are observed along with the expected (200) and (400)GaAs diffraction peaks from the GaAs substrate. There is no other peak in the diffraction profile, strongly indicating that the deposited film is single crystal with the same lattice orientation as the GaAs substrate. This was also true for all other grown InAs samples. However, thin, whisker-like growth was observed on top of the smooth surface of the InAs film grown at 350℃ as shown in Fig.5-4. These whiskers might contain wurtzite structure which is unusual for InAs and can not be detected by θ –2 θ mode XRD [8].

A SIMS depth profile measurement was performed, using O_2^+ as the primary ion beam, for the sample grown at 450℃ as shown in Fig. 5-6. A small step in the As(75) signal denotes the interface between InAs and GaAs. This step was probably caused by the matrix effect [9]. Note that As is uniformly distributed in the film. Though not shown in the figure, the elements expected to be incorporated in the film as impurities (C(12), Na(23), Si(30), Cr(52) and Fe(56)) had almost the same intensity both in the film and in the substrate. The signals of C(12), Si(30) were hardly detected.

Pihlstrom et al. reported, via SIMS analysis (using Cs^+ as the primary ion beam), significant incorporations of carbon (~ 10^{20} cm^{-3}), oxygen (10^{17}-10^{18} cm^{-3}) in the GaAs film grown using the same arsine generator [4]. Traces of Si were also detected in their GaAs films. The incorporation of oxygen and Si was attributed to the microwave H_2 plasma etching of the inner quartz wall of the arsine generator. Their GaAs was grown at the V/III ratio around 1.0 or the less and a fixed arsine flow of 0.5 sccm, both which are much lower than used in this InAs growth experiment. Simultaneously, a higher hydrogen radical flow rate was provided from the arsine generator herein. These different growth conditions probably enhanced the formation of CH_4 and C_2H_6 , reducing the carbon incorporation in the InAs film. The very low signal of Si in the InAs film can also be explained by the increased hydrogen radical effect (formation of SiH_4). The oxygen level in the InAs film is expected to be low in the similar manner.

Though the SIMS result should be analyzed very carefully, the above results show the usefulness of the plasma arsine radical generator for group III arsenide material growth, even though the etching of quartz was actually observed from frosted inner wall of the generator.

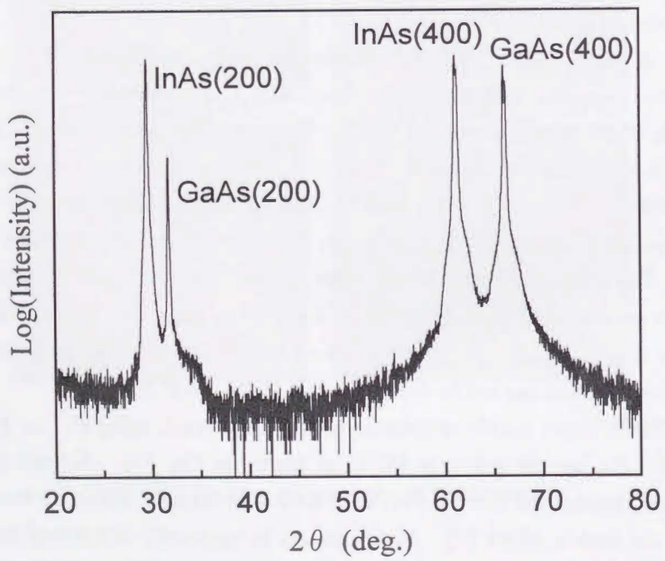

Figure 5-5. XRD profile of the InAs sample grown at 450℃.

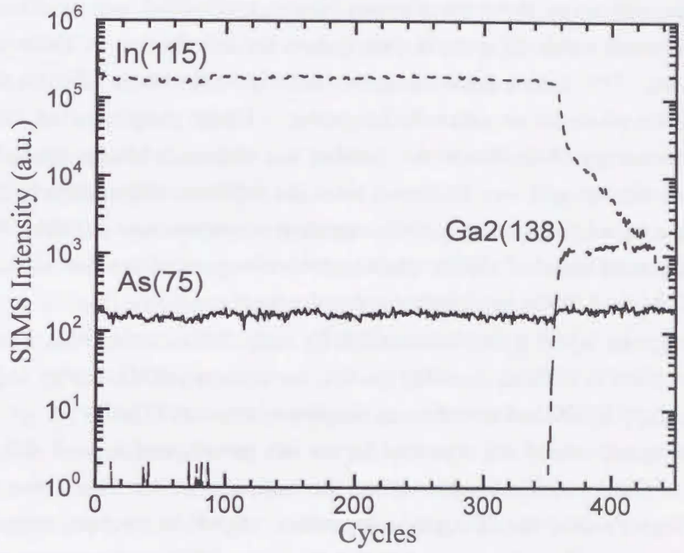

Figure 5-6. SIMS profile of the InAs sample grown at 450℃.

5-5 Growth of InNAs

5-5-1 Sample preparation and evaluation

The pre-growth substrate treatment was the same as discussed in sub-section 5-4-2, with the addition of N_2 gas flow from the beginning. After the substrate was adjusted to growth temperature, the nitrogen plasma was ignited and the microwave power was adjusted within 15 seconds, followed by the introduction of TMIn into the growth chamber. The InNAs layer was grown directly on the GaAs substrate without any pre-growth of GaAs or other buffer layers. Upon completion of the film deposition process, the TMIn flow to the chamber was stopped, while the production of arsine and atomic nitrogen was continued until the substrate temperature fell below 300℃. For simplicity, a typical growth condition is summarized in table 5-2 (the growth condition of sample CG100). InNAs with nitrogen composition of 0.13, the largest value obtained herein, was synthesized under these conditions [1].

The grown layers were characterized by x-ray diffraction (XRD), secondary ion mass spectrometry (SIMS), scanning electron microscopy (SEM), energy dispersive x-ray spectroscopy (EDX) and transmission electron microscopy (TEM).

The crystallinity of the deposited layers was investigated by a θ-2θ mode XRD with a powder diffractometer using the radiation of Cu Kα_1 and Kα_2. Assuming Vegard's law, the nitrogen composition of InNAs in each sample was determined by the lattice constant calculated from the XRD peak position without taking into account any possible effects of lattice strain. InNAs(200) diffraction peak was employed to determine the nitrogen composition because the XRD peak from InNAs(400) in each sample was too small and broad.

Table 5-2. Typical growth conditions (Sample Number: CG100).

Substrate	2° off GaAs(100)
Growth Temperature	500℃
TMIn	0.141 sccm
In situ Generated Arsine	0.53 sccm
N_2, Microwave Power	100 sccm, 70 W
H_2(total)	225 sccm
Pressure	750 mTorr
Growth Duration	60 minutes

5-5-2 Growth at different temperatures

Figure 5-7 shows XRD profiles of the samples grown in the temperature range of 450-550℃. All other growth conditions are the same as in table 5-2. The thicknesses of the deposited layers are 200, 150, 150 and 70 nm for the growth temperatures of 450, 475, 500 and 550℃ respectively. This decrease in the growth rate is probably due to the enhanced etching effect of the depositing layer by hydrogen radicals as well as the enhanced desorption of the feed species from the substrate at higher growth temperatures, because the growth rate of InN (without production of hydrogen plasma) increased with increasing the growth temperature from 450℃ (130 nm/hour) to 550℃ (350 nm/hour). The two large peaks around 31.7° and 66.0° in each XRD profile are from the GaAs substrate. For the sample grown at 450℃, only the peaks from wurtzite phase InN can be seen. As for the sample grown at 475℃, a very small peak from InNAs(200) is observed around 30° . The nitrogen composition of the 475℃ InNAs was not precisely determined due to the small, broad nature of the peak. Further increse in the growth temperature results in more intense (200) and (400)InNAs diffraction peaks. However, the resultant InNAs(200) peak position shifts to the smaller 2θ values from 30.21° (500℃) to 29.88° (550℃), i.e. the nitrogen composition of InNAs decreases from 13% (500℃) to 7% (550℃). This is explained by the lower N solubility at higher growth temperatures [10-15]. A SIMS depth profile measurement, using O_2^+ as the primary ion beam, was performed to investigate Ga diffusion from the substrate into the deposited layer which might cause an over-estimation for the nitrogen content of InNAs. Figure 5-8(a) shows the depth profile for sample CG100. It is clear that Ga is not considerably incorporated in the deposited layer. The As(75) signal is very weak in the grown layer. This is because the main component of the deposited layer is InN and the SIMS sensitivity to arsenic atom is low. Hence, InNAs grown at 500℃ is confirmed. However, a considerable amount of Ga from the substrate was observed for sample CG102, as shown in Fig. 5-8(b), probably due to the enhanced Ga diffusion at relatively high growth temperatures. The nitrogen content of (Ga)InNAs in CG102 is 7% in the author's estimation. A picture of the surface morphology taken by an optical microscope is shown in Fig. 5-9 for sample CG100. It is possible that the incorporation of As atoms from the substrate into the InNAs phase might take place. Depositions without arsine production (i.e., the growth of InN) were performed at 450, 500 and 550℃. TMIn was introduced into the growth chamber as soon as the microwave power for arsine production was turned off, while hydrogen gas flowed through the arsine generator during the growth. The XRD profiles of these samples included the peaks from only

wurtzite phase InN along with the expected (200) and (400)GaAs diffraction peaks from the substrate. These profiles were similar to that of sample CG101 shown in Fig. 5-7, revealing that the arsenic atoms in the InNAs phase were incorporated from the vapor phase (Additional evidence is given by changing the arsine flow rate, which is shown in sub-section 5-5-4.).

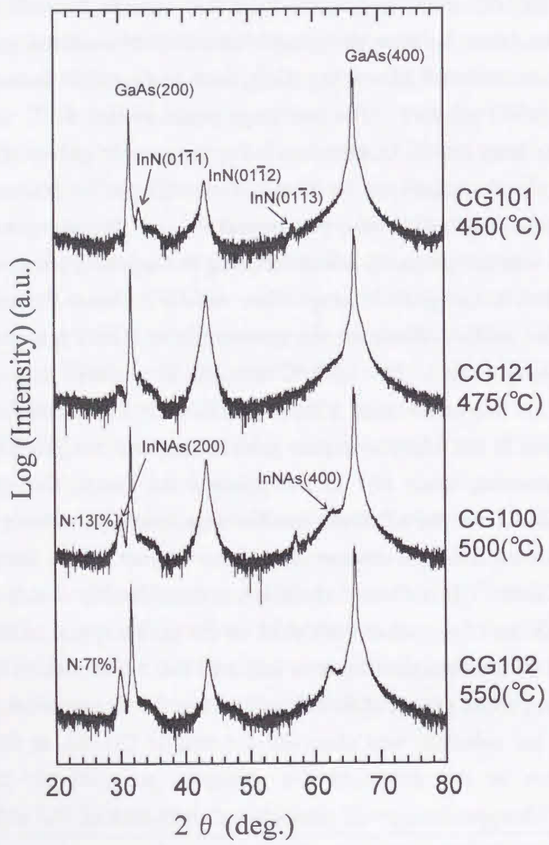

Figure 5-7. XRD of the samples grown at different temperatures.

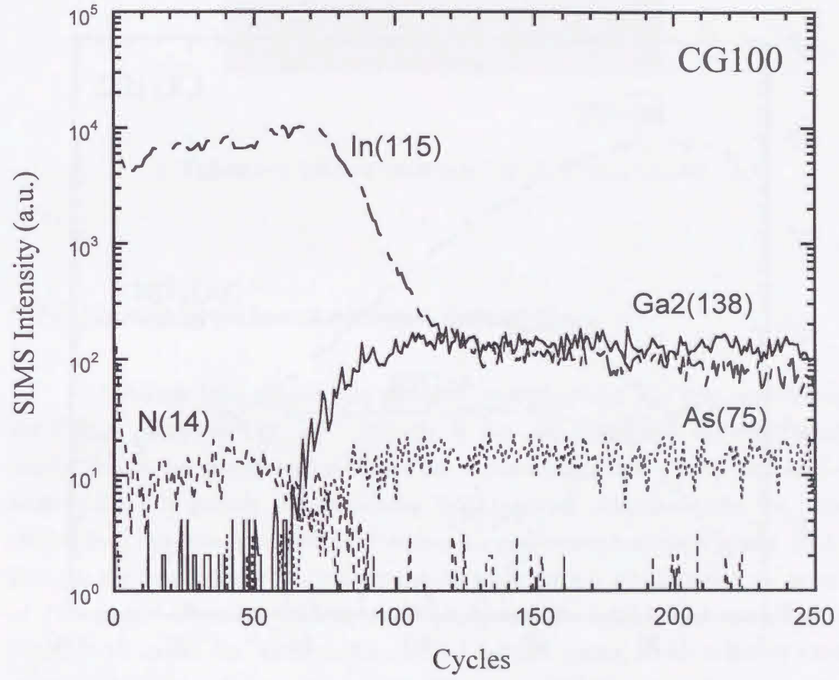

Figure 5-8(a). SIMS profile of the sample CG100 grown at 500℃.

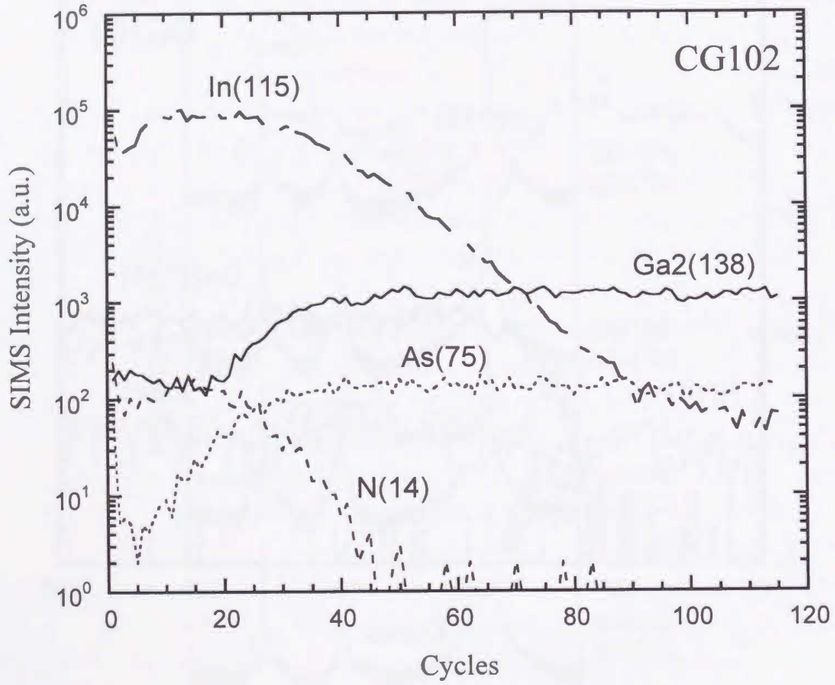

Figure 5-8(b). SIMS profile of the sample CG102 grown at 550℃. The grown layer was thinner than CG100, the profile was taken in short depth range.

Figure 5-9. Surface micrograph of the sample CG100.

5-5-3 Growth at different nitrogen radical flows

Although $InN_{0.13}As_{0.87}$ was obtained, wurtzite phase InN was predominant in the film as shown in Fig. 5-7. Initially, it was speculated that too much nitrogen radical flow to the growth region caused the wurtzite phase InN. With the intention of suppressing InN growth and enhancing InNAs growth simultaneously, the nitrogen radical flow rate was decreased by lowering the microwave excitation power, while the nitrogen gas flow through the nitrogen radical generator was maintained at the same rate of 100 sccm. The other growth conditions were the same as for sample CG100. Figure 5-10 shows the XRD profiles of the samples grown at the different nitrogen source microwave powers. The profile for sample CG100 in Fig. 5-7 is reprinted in Fig. 5-10 for a systematic comparison of the XRD data. At the nitrogen source microwave excitation power of 50 W, the XRD peaks of InNAs are larger than at 70 W. However, the nitrogen composition of InNAs decreases to 7% while the large InN($01\bar{1}$ 2) peak is almost the same intensity. At the reduced microwave power of 30 W, the peak from InN($01\bar{1}2$) becomes smaller. However, the diffraction peaks from (200) and (400)InAs begin to appear, leaving the InNAs diffraction shoulders on their peaks. A very small peak from zincblende phase InN can be seen around 36.2° . Though not shown in the figure, further decrease in microwave power eliminated the diffraction peaks from ($01\bar{1}2$) and (200)InN (at 10 W), and the diffraction around 39.1° from In(200) began to appear. When the microwave power was decreased down to 0 W

(with the nitrogen gas flow rate of 100 sccm through the radical generator maintained), the In(200) peak grew stronger, and the small diffraction peaks from (111) and (002)In were observed around 33.0° and 36.5° respectively. The resultant (200) and (400)InAs diffraction peaks became much broader with large tails toward the GaAs peaks, probably due to the enhanced interdiffusion of Ga and In at the interface between the deposited layer and the substrate. These results clearly indicate that the effective source ratio of As/In in the growth region was less than unity, which seems to be an advantage for single-crystal growth of InNAs with a high nitrogen composition. However, the excess In, under a sufficient nitrogen radical ambient, might easily form the InN phase in the depositing layer.

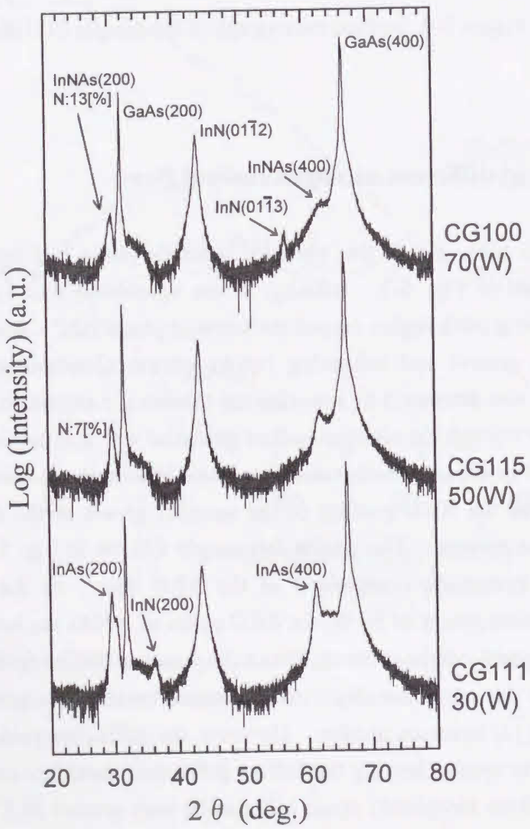

Figure 5-10. XRD of the samples grown at different N_2-cracking microwave powers.

5-5-4 Growth at different arsine radical flows

The arsine flow rate was raised to 1.05 sccm by increasing the H_2 flow through the arsine radical generator. Accordingly, the total H_2 flow into the growth chamber was increased. The other growth conditions were the same as that for sample CG100. The resultant XRD patterns appeared almost the same as that of sample CG100 (see Fig. 5-7 or Fig. 5-10), while the InNAs peak position shifted to the smaller 2θ with increase in the arsine flow rate. The XRD intensities of the InN(01$\bar{1}$2) and InNAs(200), (400) peaks stayed almost constant, without any systematic relationship to the arsine flow rate. The arsine flow rate vs. the nitrogen composition as well as the arsenic composition of the InNAs phases is shown in Fig. 5-11. Though only three points of data are obtained in the experiment, the arsenic composition does not seem to increase linearly with increase in the arsine flow rate, instead appearing to saturate at higher arsine flow rates. This behavior of the arsenic composition is similar to that of most mixed group V ternary alloys (e.g., $InAs_xSb_{1-x}$ [16], InP_xAs_{1-x} [17]), though it is difficult to evaluate the relative composition rate constant of As (or N) to N (or As) for the InNAs phase because InN is also contained in the deposited layer. The nitrogen radical flux was not estimated.

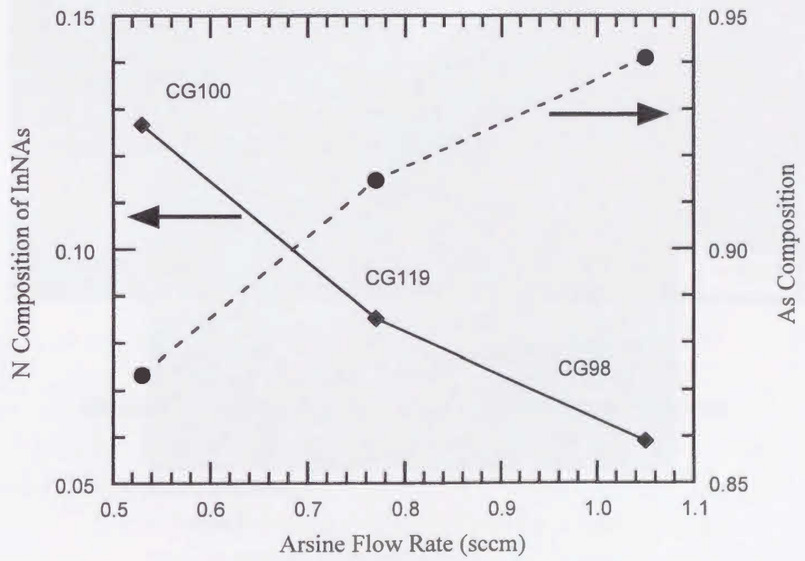

Figure 5-11. N and As composition in InNAs phase as a function of arsine flow rate. The lines are used only to guide the eye.

5-5-5 Distribution of InNAs phase in the grown layer

For sample CG100, the growth duration was reduced to 10 minutes. The InNAs(200) XRD peak always stayed at the same 2θ value. The XRD peak intensities of $InN_{0.13}As_{0.87}$(200) and InN($01\bar{1}2$) monotonically increased with increasing growth duration, maintaining a constant ratio of the I($InN_{0.13}As_{0.87}$) / I(InN) intensities. This indicated a uniform distribution of the InNAs phase in a matrix of wurtzite phase InN. Figures 5-12(a) and (b) show a SEM surface image and a TEM cross-sectional image of CG100, respectively. For the surface image, energy dispersive x-ray spectroscopy (EDX) mapping as well as a line-scan of As La1 were carried out. However, the As signal was very weak and the profiles were noisy, so the InNAs layers were not distinguished. For the cross-sectional image, selected area (including the substrate) electron diffraction was measured. The diffraction from the area always contained more than two patterns except from the substrate, and the patterns were complicated as shown in Fig. 5-12(c). It could not be distinguished which diffraction was from InNAs phase. These failures in the measurements were probably due to the very small volume of each InNAs grain.

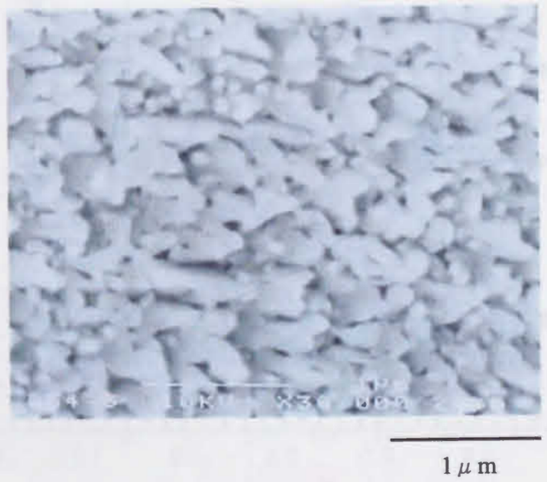

Figure 5-12(a). SEM surface image of the sample CG100.

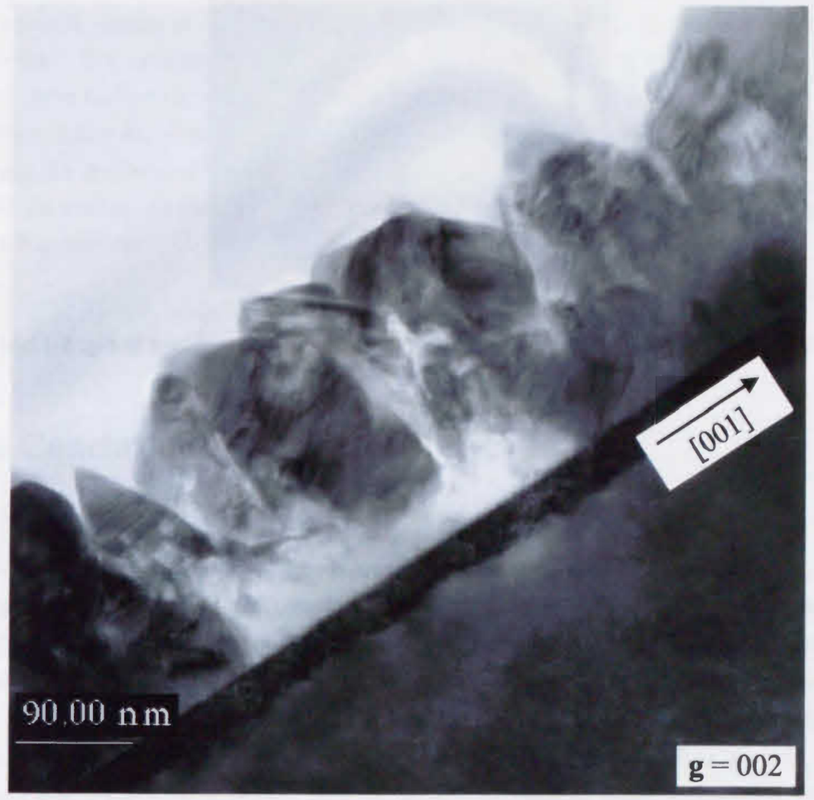

Figure 5-12(b). TEM cross-sectional image of the sample CG100.

Figure 5-12(c). [010] electron diffraction pattern from an area shown in Fig. 5-12(b).

Fourier transformation infrared spectroscopy (FTIR) measurement was performed for all the InNAs samples, using a clean GaAs substrate or InN/GaAs substrate as a reference. However the resultant transmission spectra from the grown layers were all flat. These results can also be explained by the small volume of InNAs grains.

5-5-6 Discussion

The growth of InNAs was always accompanied by growth of wurtzite phase InN with the $(01\bar{1}2)$ planes parallel to the surface as shown in Fig. 5-7 and Fig.5-10. Recently, single crystalline wurtzite GaN films were grown on vicinal (100)GaAs substrates by plasma-assisted MBE using a radio frequency nitrogen plasma source [18]. The $(01\bar{1}2)$ planes were parallel to the surface and the diffraction plane was identified as GaN$(10\bar{1}2)$, which is equivalent to GaN$(01\bar{1}2)$. The above author used the nitridation of the GaAs surface before the growth. High resolution TEM observation proved that

the layer was grown with the [0001] direction (c axis) inclined to the surface normal by 43° (the angle between the wurtzite $(01\bar{1}2)$ and (0001) GaN planes). The single crystalline zincblende GaN layers were also grown under the above author's unique growth conditions using a stoichiometric N/Ga flux ratio and without nitridation of the GaAs surface. It is speculated that the same effects could occur during the growth of InN. In growth experiments of InNAs (and InN) herein, the substrate was exposed to the nitrogen plasma as well as the arsine radicals for 15 seconds just before growth initiation. The exposure to nitrogen radicals prior to the onset of film growth might cause some surface nitridation, leading to the favorable formation of wurtzite InN with the same lattice orientation relationship as that of wurtzite GaN in Ref. [18], and hence, prevent the synthesis of single crystalline zincblende InNAs layer. A careful effort to avoid the surface nitridation seems to be necessary before investigating the optimum growth conditions

5-6 Conclusions

Plasma-cracked nitrogen, in situ generated arsine radicals and TMIn were introduced separately into the MOCVD growth chamber at a reduced pressure of 750 mTorr to avoid the gas phase chemical reactions among the source species or the formation of any possible polymers. InN_xAs_{1-x} (x = 0.06～0.13) phases were grown on vicinal GaAs(100). Single crystalline InAs films were also obtained using the same arsine source, without any significant incorporation of impurities. The growth of InNAs was always accompanied with the growth of wurtzite phase InN, which was attributed to nitridation of the GaAs surface before the growth process. The grown InNAs layers were expected to be very small grains uniformly distributed in the matrix of wurtzite InN. The nitrogen composition of InNAs increased with increase in the nitrogen radical flow rate and decreased with increase in the arsine flow rate. Increasing the growth temperature reduced the nitrogen composition of InNAs, explained by the lower N solubility at higher growth temperature. It is suggested that not only the adjustment of each growth condition but also a careful effort to avoid the nitridation of GaAs surface before the deposition process is necessary for the film growth of single crystalline InNAs.

References

[1] H. Naoi, D. M. Shaw, Y. Naoi, G. J. Collins and S. Sakai: J. Cryst. Growth (in press).

[2] H. Naoi, D. M. Shaw, G. J. Collins and S. Sakai: J. Cryst. Growth **219**, (2000) 481.

[3] F. C. Fehsenfeld, K. M. Evenson and H. P. Broida: Rev. Sci. Instr. **36**, (1965) 294.

[4] B. G. Pihlstrom, L. R. Thompson, D. M. Shaw, A. D. Simone, T. Y. Sheng, J. Lurkins and G. J. Collins: J. Electron. Mater. **22**, (1993) 81.

[5] B. G. Pihlstrom, T. Y. Sheng, L. R. Thompson and G. J. Collins: J. Electron. Mater. **21**, (1992) 277.

[6] K. Y. Ma, Z. M. Fang, R. M. Cohen and G. B. Stringfellow: J. Electron. Mater. **21**, (1992) 143.

[7] See, for example, G. B. Stringfellow: *Organometallic Vapor-Phase Epitaxy: Theory and Practice*, 1st edition (Academic Press, San Diego, 1989) pp. 145, 158-160 (Chapter 4).

[8] M. Koguchi, H. Kakibayashi, M. Yazawa, K. Hiruma and T. Katsuyama: Jpn. J. Appl. Phys. **31**, (1992) 2061.

[9] See, for example, Hyoumen Bunseki Gijyutu Sensho: *Niji-ion Sitsuryou Bunseki-hou (SIMS)*, 1st edition, The Surface Science Society of Japan (1999) [in Japanses].

[10] S. Miyoshi, H. Yaguchi, K. Onabe, Y. Shiraki and R. Ito: Jpn. J. Appl. Phys. **36**, (1997) 7110.

[11] S. Miyoshi, H. Yaguchi, K. Onabe, R. Ito and Y. Shiraki: Appl. Phys. Lett. **63**, (1993) 3506.

[12] W. G. Bi and C. W. Tu: Appl. Phys. Lett. **69**, (1996) 3710.

[13] M. Weyers and M. Sato: Appl. Phys. Lett. **62**, (1993) 1396.

[14] K. Uesugi and I. Suemune: J. Cryst. Growth **189/190**, (1998) 490.

[15] W. G. Bi and C. W. Tu: J. Appl. Phys. **80**, (1996) 1934.

[16] T. Fukui and Y. Horikoshi: Jpn. J. Appl. Phys. **19**, (1980) L53.

[17] T. Fukui and Y. Horikoshi: Jpn. J. Appl. Phys. **14**, (1980) L551.

[18] K. Amimer, A. Georgakilas, K. Tsagaraki, M. Androulidaki, D. Cengher, L. Toth, B. Pecz and M. Calamiotou: Appl. Phys. Lett. **76**, (2000) 2580.

Chapter 6
Summary

In this doctoral study, growth of InNAs was studied by several deposition methods and the following works have been performed.

In chapter 1, the fundamental properties and recent progress of III-N-V alloys as well as the present research situation of InNAs were briefly summarized.

In chapter 2, the growth of InNAs by conventional MOCVD using NH_3 as the nitrogen source was presented. All the grown InNAs layers were island grown and had direct transition band structures. The band gap energy decreased with increase in the nitrogen solid phase composition as expected. The nitrogen solid phase composition of InNAs could be increased up to 0.061, and the band gap energy of $InN_{0.061}As_{0.939}$ appeared around 0.12 eV. Only 6.1% of nitrogen into InAs was shown to produce a narrow band gap energy comparable to the minimum band gap of 0.10 eV achieved by $InAs_xSb_{1-x}$ material system among all the conventional III-V semiconductors. The low nitrogen composition of the grown InNAs was explained by low pyrolysis efficiency of ammonia in the range of InNAs growth temperatures.

In chapter 3, the results of layers grown by plasma-assisted MOCVD performed at 3 Torr were presented. In this MOCVD system, all the mixed source gases were cracked by microwave excitation upstream of the growth substrate in an attempt to grow InNAs with the higher nitrogen composition and with good compositional uniformity. No crystallized InNAs was obtained using this method. The growth of InN was also performed. The grown InN films were almost amorphous with the zincblende phase in a slight majority. These poor results were attributed to gas phase chemical reactions between activated source species. The necessity of separate production and introduction of nitrogen radicals into the growth chamber at reduced pressure was pointed out.

In chapter 4, it was demonstrated that an InNAs layer could be grown by MBE

by adjusting the flux ratio of N/As so that the grown layer was nearly lattice-matched to the GaAs substrate. The InNAs layer grown had a rough surface and included phase-separated InAs.

In chapter 5, the growth of InNAs by employing the separate production of nitrogen radicals and its separate introduction into an MOCVD growth chamber at a reduced pressure of 750 mTorr was presented. In this MOCVD system, a plasma arsine generator that provides a low production rate of arsine radicals was used to increase the N/As source ratio with the goal of synthesizing InNAs with a high nitrogen solid phase composition. InN_xAs_{1-x} (x = 0.06~0.13) phases were obtained. Single crystalline InAs films were also obtained using the same arsine source. The grown InNAs layer was always accompanied by wurtzite InN. The occurrence of the phase-separated InN was attributed to nitridation of the GaAs surface before the growth process.

List of publications

"X-ray photoelectron spectroscopy of zinc blende InN and valence-band discontinuity in the heterojunction InN/GaAs"
Proceedings of International Symposium on Blue Laser and Light Emitting Diodes, 1996, pp. 504-505.
Tao YANG, Yoshiki NAOI, Hiroyuki NAOI and Shiro SAKAI

"MOCVD growth of InAsN for infrared applications"
Solid State Electronics **41**, (1997) 319.
Hiroyuki NAOI, Yoshiki NAOI and Shiro SAKAI

"Growth of InNAs on GaAs(100) substrates by molecular-beam epitaxy"
Journal of Crystal Growth **189/190**, (1998) 471.
Shiro SAKAI, Tin S. CHENG, Thomas C. FOXON, Tomoya SUGAHARA, Yoshiki NAOI and Hiroyuki NAOI

" Heteroepitaxial growth of InAs by low-pressure metalorganic chemical vapor deposition employing in situ generated arsine radicals"
Journal of Crystal Growth **219**, (2000) 481.
Hiroyuki NAOI, Denis M. SHAW, George J. COLLINS and Shiro SAKAI

"Growth of InNAs by low-pressure metalorganic chemical vapor deposition employing microwave-cracked nitrogen and in situ generated arsine radicals"
Journal of Crystal Growth (in press).
Hiroyuki NAOI, Denis M. SHAW, Yoshiki NAOI, George J. COLLINS and Shiro SAKAI

"Growth of InAs on GaAs(100) by low-pressure metalorganic chemical vapor deposition employing in situ generated arsine radicals"

Journal of Crystal Growth (in preparation).

Hiroyuki NAOI, Denis M. SHAW, Yoshiki NAOI, George J. COLLINS and Shiro SAKAI

様式9

論文審査の結果の要旨

報告番号	甲　工 乙　工　第　185　号 工　修	氏　名	直井　弘之
審査委員	主　査　　酒井士郎 副　査　　新谷義廣 副　査　　金城辰夫		

学位論文題目

Growth and Characterization of InNAs

審査結果の要旨

本論文は、新しい半導体材料である窒化III-V 族半導体、特にInNAs の成長と評価に関わるものである。

第一章のイントロダクションに続き、第二章では、アンモニアとTMGa を原料とした通常のMOCVD によりInNAs 結晶が得られた結果が述べられている。第三章ではプラズマ分解した窒素を原料とする成長法についての初期的実験結果が述べられている。第四章ではMBE法で成長したInNAs の結果が述べられている。第五章は、本論文の中心となる部分で、装置内で合成したAsH3 とプラズマ分解した窒素を原料とする成長法について述べられている。最初にInAs の成長を実証して装置内で合成したAsH3 が半導体結晶成長に有用であることを実証した後、InNAs の成長を行い、その成長に成功している。最後に第六章では、本研究で明らかとなった点がまとめられている。

以上、本研究は、色々な手法でInNAs 結晶成長を試みたものである。本研究より以前には、この結晶の成功例はほとんど無く、パイオニア的な研究と言える。以上のことから、本論文は博士（工学）の学位授与に値するものと判定する。